Chapter 2
Friction and Wear

Pradeep L. Menezes, Michael Nosonovsky, Satish V. Kailas, and Michael R. Lovell

Abstract Friction is a universal phenomenon which is observed in a great variety of sliding and rolling situations. The study of friction and wear has long been of enormous practical importance, since the functioning of many mechanical, electromechanical, and biological systems depends on the appropriate friction and wear values. In recent decades, this field has received increasing attention as it has become evident that the consumption of resources resulting from high friction and wear is greater than 6 % of the Gross National Product of the USA. In this chapter, various theories, mechanisms, and factors affecting of friction and wear were discussed.

1 Introduction

Friction plays a great role in the everyday life. Without friction it would be impossible to walk, use automobiles on a roadway, or pick up objects. In various situations, either low or high friction may be desirable. For example, in some machine applications such as vehicle brakes and clutches and frictional transmission of power, high friction is needed. However, in most other sliding and rolling components such as bearing and seals, friction is undesirable. Friction causes energy loss and the wear of materials that are in contact. In these cases, friction should be minimized.

P.L. Menezes (✉) • M. Nosonovsky • M.R. Lovell
College of Engineering & Applied Science, University of Wisconsin-Milwaukee, Milwaukee, WI 53201, USA
e-mail: menezesp@uwm.edu

S.V. Kailas
Department of Mechanical Engineering, Indian Institute of Science, Bangalore, Karnataka 560012, India

P.L. Menezes et al. (eds.), *Tribology for Scientists and Engineers: From Basics to Advanced Concepts*, DOI 10.1007/978-1-4614-1945-7_2,

2 Friction

Friction is the resistance to relative motion of two bodies that are in contact. Friction is not a material property; it is a property of tribological system that consists of at least two bodies in contact, along with the surrounding environment and the interface. There are two types of friction that are commonly encountered: dry friction and fluid friction. Dry friction is also called "Coulomb" friction. Dry friction occurs during the contact under dry conditions, while the fluid friction occurs during the contact under lubricated conditions. If two solid surfaces are smooth and clean without chemical films and adsorbates, friction is usually high. Surface contaminants or thin films affect friction. With well-lubricated surfaces, low friction is generally observed.

2.1 Basic Concepts

2.1.1 Coefficient of Friction

Friction can often be described by a quantitative parameter called the coefficient of friction, μ. It is known from experiments that the friction force is often linearly proportional to the normal load force applied to the body. This is the so-called Coulomb friction. The coefficient of friction, also known as friction coefficient, is a dimensionless scalar value defined as the ratio of tangential friction force (F) to the normal load force (W).

$$\mu = \frac{F}{W} \tag{2.1}$$

As illustrated in Fig. 2.1, a tangential force (F) is needed to move the upper body over the stationary counterface. As explained above, the ratio between these two forces is known as the coefficient of friction.

In technical terms, friction force or tangential force is the resisting force which acts in a direction directly opposite to the direction of motion. The normal force is defined as the net force compressing two parallel surfaces together, and its direction is perpendicular to the surfaces. In the simple case of a mass resting on a horizontal

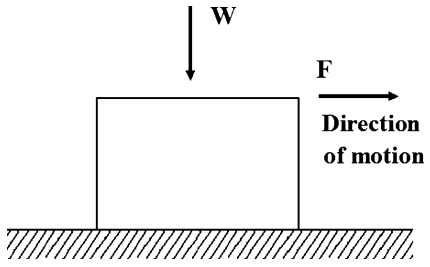

Fig. 2.1 Schematic diagram of a body sliding on a surface

surface, the only component of the normal force is the weight force due to gravity. In this case, the maximum magnitude of the friction force is the product of the mass of the object, the acceleration due to gravity, and the coefficient of friction. However, the coefficient of friction is not a function of mass or volume; it depends only on the mating materials and testing conditions. For instance, a large aluminum block in contact with steel has the same coefficient of friction as a small aluminum block contacting steel. However, the magnitude of the friction force itself depends on the normal force and hence the mass of the block.

The coefficient of friction is an empirical parameter—it has to be measured experimentally and cannot be found through calculations. The coefficient of friction can vary over a wide range: from 0.001 in a lightly loaded rolling bearing to greater than 10 for clean metals sliding against themselves in vacuum. For most common materials, sliding in air, the value of the coefficient of friction lies in the narrower range from about 0.1 to 1.

2.1.2 Static Friction

Static friction is the friction between two solid objects that are not moving relative to each other. For example, static friction can prevent an object from sliding down a sloped surface. The coefficient of static friction, typically denoted as μ_s, is usually higher than the coefficient of kinetic friction, μ_k. This happens because when no sliding occurs, the surfaces tend to "stick" to each other due to adhesive bonds between them. This phenomenon is sometimes referred to as "stiction." The static friction force must be overcome by an applied force before an object can move. The instant of sliding occurs, static friction is no longer applicable, and kinetic friction becomes applicable.

2.1.3 Kinetic Friction

Kinetic (or dynamic) friction occurs when two bodies are moving relative to each other and rub each other. The coefficient of kinetic friction is typically denoted as μ_k and is usually less than the coefficient of static friction for the same material combination. Figure 2.2 demonstrates the static and kinetic friction with time.

2.1.4 Angle of Friction

For certain applications, it is more useful to define static friction in terms of the maximum angle before which one of the items will begin sliding. This is called the *angle of friction* or *friction angle*. It is defined as

$$\tan\theta = \mu \tag{2.2}$$

where θ is the angle from horizontal and μ is the static coefficient of friction between the objects.

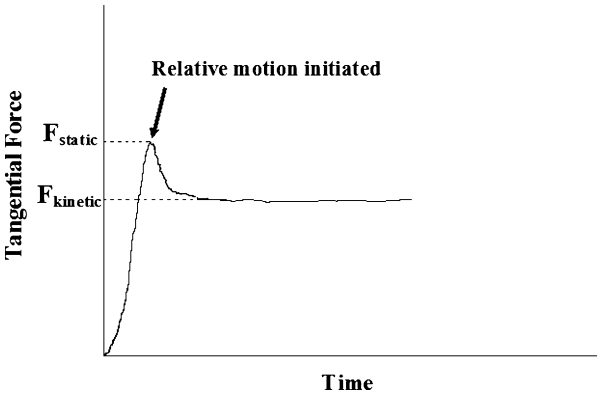

Fig. 2.2 Variation of tangential force with time. F_{static} is the force required to initiate sliding and $F_{kinetic}$ is the force required to maintain sliding

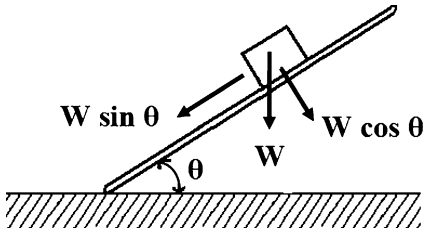

Fig. 2.3 Measurement of friction using the inclined plane test

Consider a block of weight W is placed upon an inclined plane of angle θ to the horizontal as shown in Fig. 2.3, the coefficient of friction can be defined as

$$\mu = \frac{F}{W} = \frac{W \sin\theta}{W \cos\theta} = \tan\theta \tag{2.3}$$

In (2.2), θ is the angle such that a body of any weight, placed on a plane inclined at an angle less than θ from the horizontal, will remain stationary. However, if the inclination angle is increased to θ, the body will start to slide down. This formula can also be used to calculate μ from empirical measurements of the friction angle.

2.1.5 Stick–Slip Phenomenon

An important phenomenon during sliding is the stick–slip motion. During the stick–slip motion, the frictional force does not remain constant, but rather oscillates significantly as a function of sliding distance or time. During the stick phase, the friction force builds to a critical value. Once the critical force has been attained (to overcome the static friction), slip occurs at the interface and energy is released so that the frictional force decreases. This stick–slip phenomenon can occur if the coefficient of static friction is greater than the coefficient of kinetic friction [1].

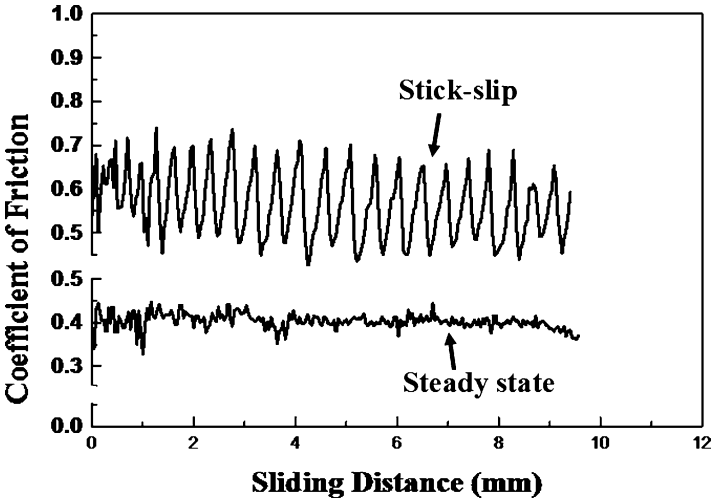

Fig. 2.4 Variation of steady-state and stick–slip friction with sliding distance

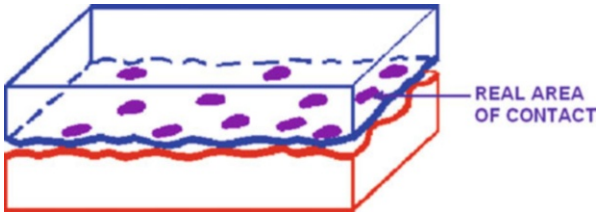

Fig. 2.5 Schematic view of real area of contact between two bodies

Figure 2.4 shows the variation of steady-state motion and stick–slip motion with sliding distance [2].

The stick–slip phenomenon is found in many situations, such as car brake vibration and squeal. However, it is particularly common at the atomic scale. For example, during the contact of an atomic force microscope tip with an atomically smooth surface, the energy dissipation takes place through stick–slip movement of individual atoms at the contact interface [3].

2.1.6 Real Area of Contact

Even nominally flat surfaces are not perfectly smooth and have asperities at some length scale. When two surfaces are brought into contact, the contact occurs only at the tops of the asperities, so the load is supported by the deformation of contacting asperities. Therefore, the real (or actual) area of contact constitutes only a small fraction of the nominal (or apparent) area of contact. Figure 2.5 shows the real area of contact, schematically. In general, the real area of contact varies with the pressure and is very small compared to the nominal area of contact. For flat steel

surfaces under typical loads, the real area of contact may be less than 0.01 % of the apparent area. The real area of contact is not greatly affected by the size, shape, and degree of roughness of the surface; it depends mainly on the pressure. However, during sliding locations of the contact spots do not remain permanent, but are changing rapidly during sliding, as new asperities come into contact while other contacts break.

2.1.7 Friction Paradoxes and Dynamic Instabilities

Despite the linear dependence of the Coulomb friction force upon the normal load given by (2.1), friction is an inherently nonlinear phenomenon. Direction of the friction force depends upon the direction of motion, so that in the vector form, the friction force is given by

$$\vec{F} = \frac{\vec{V}}{\left|\vec{V}\right|}\mu\left|\vec{W}\right| \tag{2.4}$$

where $\vec{V}$ is the sliding velocity. The ratio $\vec{V}/|\vec{V}|$ is nonlinear. This nonlinearity results in some static frictional problems having no solution or a nonunique solution, e.g., the so-called Painlevé paradoxes. These paradoxes show that the rigid-body dynamics with contact and Coulomb friction is inconsistent. To resolve these problems, the dynamic friction and elastic deformation should be considered [3].

Despite the simplicity of (2.1) to describe friction, there are a number of difficulties in integrating friction with the mechanics of a deformable body. In continuum mechanics, stress is the measure of force exerted per unit area at a given point. The maximum shear stress τ_{xy} at the interface between two bodies during friction is proportional to the normal stress σ_{yy} at the same point

$$\tau_{xy} = \mu\sigma_{yy} \tag{2.5}$$

However, the sign of the shear stress depends upon the sign of the local sliding velocity. This leads to friction paradoxes when formal mathematical solutions of the continuum mechanics problems with the boundary condition given by (2.3) yield nonunique solution or to the sign of the shear stress not necessarily opposite to the sign of the local velocity of sliding. Adams et al. [4] demonstrated that dynamic effects lead to new types of frictional paradoxes, in the sense that the assumed direction of sliding used for Coulomb friction is opposite that of the resulting slip velocity. In a strict mathematical sense, the Coulomb friction is inconsistent not only with the rigid-body dynamics (the Painlevé paradoxes) but also with the dynamics of elastically deformable bodies.

The mathematical formulation of quasi-static sliding of two elastic bodies (half-spaces) with a frictional interface, governed by (2.4), is a classical contact mechanics problem. Interestingly, the stability of such sliding has not been

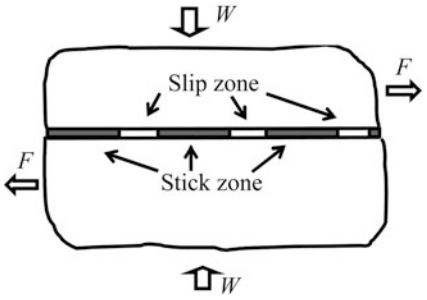

Fig. 2.6 Friction reduction due to propagating stick–slip zones

investigated until the 1990s, when Adams [5] showed that the steady sliding of two elastic half-spaces is dynamically unstable, even at low sliding speeds. The instability mechanism is essentially one of slip-wave destabilization. Steady-state sliding was shown to give rise to a dynamic instability in the form of self-excited motion. These self-excited oscillations are confined to a region near the sliding interface and can eventually lead to either partial loss of contact or to propagating regions of stick–slip motion (slip waves). The existence of these instabilities depends upon the elastic properties of the surfaces; however, it does not depend upon the friction coefficient, nor does it require a nonlinear contact model. The same effect was predicted theoretically by Nosonovsky and Adams [6] for the contact of rough periodic elastic surfaces.

The abovementioned instabilities are a consequence of energy being pumped into the interface as a result of the positive work of the driving force (that balances the friction force). As a result, the amplitude of the interface waves grows with time. In a real system, of course, the growth is limited by the limits of applicability of the linear elasticity and linear vibration theory. This type of friction-induced vibration may be, at least partially, responsible for noise and other undesirable effects during friction [6]. These instabilities are a consequence of the inherent nonlinearity of the boundary conditions with the Coulomb friction. The stick–slip phenomenon is another important nonlinear effect similar to the dynamic instability due to decrease of friction force with increasing velocity.

Another important dynamic effect is the slip waves that can propagate along a frictional interface between two bodies. The slip wave is a propagating stick–slip motion. In a slip wave, a region of slip propagates along the interface, which is otherwise at the stick state (Fig. 2.6). As a result, two bodies shift relative to each other in a "caterpillar" or "carpet" motion at a shear force F smaller than μW, effectively resulting in the decrease of the apparent coefficient of friction. The concept of the slip waves has been applied in seismology for the study of the motion of earth plates as well as in the solid state physics for the gliding of the dislocation at an interface between two bodies [7].

When the interface waves occur for slightly dissimilar (in the sense of their elastics properties) materials, waves for very dissimilar materials would be radiated along the interfaces to provide a different mechanism of pumping the energy away from the interface [8].

2.1.8 Time-Dependent Friction

It is known from experiments that the absolute value of the friction force is not completely independent of the sliding velocity. In fact, it has been known already to Coulomb, who claimed that for very small velocities friction force grows with increasing velocity, for moderate velocities friction force remains constant, and for high velocities it decreases. It is known from experiments also the normal degree of freedom plays an important role in many dynamic effects [9]. The separation distance between the sliding bodies grows with increasing velocity. At high sliding velocities there is less time for the individual asperity contacts and, therefore, less time for asperities to deform (e.g., viscoplastically). This usually results in a decrease of the real area of contact and decrease of the friction force with increasing velocity. Various dynamic models have been suggested, based on various physical effects, such as time-dependent creep-like relaxation and viscosity [10].

It is usually believed that increasing velocity in dry friction results in decreasing friction (the so-called negative viscosity), although for some material combinations and friction regimes, the opposite trend is observed. Note that the decrease of friction with increasing velocity may lead to a dynamic instability since decreased frictional resistance will lead to acceleration and further increase of velocity and decrease in friction.

To analyze frictional dynamic instabilities (DI), the so-called state-and-rate models of friction have been introduced [10–12]. These models, used at first to study sliding friction for seismic and geophysical applications, showed reasonable agreement with the experimental data. Based on the state-and-rate models, when sliding velocity changes, the friction force first increases and then decreases (due to creep relaxation) to a velocity-dependent steady-state value (which, itself, is dependent upon the sliding velocity).

Another type of instability is a result of interaction between frictional heating, thermoelastic distortion, and contact pressure and known as the “thermoelastic instability” (TEI). As the interface temperature grows, the near-surface volumes of the contacting bodies expand and the contact pressure grows. As a result, the friction force increases as well resulting in excess heat generation and the further growth of the temperature. The TEI leads to the formation of “hot spots” or localized high-temperature regions at the interface [13]. The TEI occurs for sliding velocities greater than a certain critical value. The coupling between the two types of instabilities constitutes thermoelastodynamic instability (TEDI). Another mechanism that may provide instability is the coupling between friction and wear. As friction increases, so does the wear, which may result in an increase of the real area of contact between the bodies and in further increase of friction. The sliding bodies adjust to each other, and the process is known as the frictional self-organization [14, 15]. On the other hand, wear produces smoothening of the surface distorted by the TEI mechanism, and thus the wear and thermal expansion are competing factors, with the wear leading to stabilization of sliding and the thermal expansion leading to destabilization (Fig. 2.7).

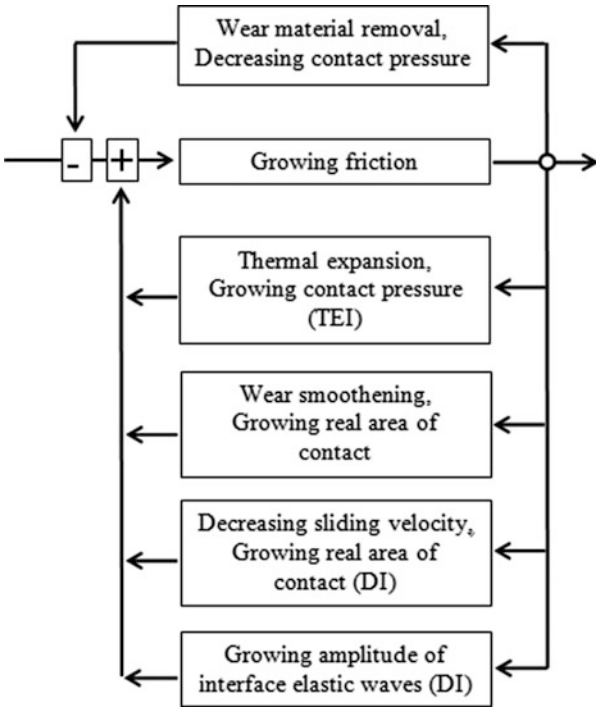

Fig. 2.7 Various mechanisms can create positive or negative feedbacks that lead to instabilities during friction

2.1.9 Self-Organization During Friction

Sliding friction does not always lead to wear and deterioration but has potential for self-organization. This is because friction is a nonequilibrium process that results in the dissipation of large amounts of energy and in the flow of heat, entropy, and material away from the frictional interface. It is well known that when the sliding starts friction and wear are usually high during the initial "run-in" regime. However, with time the surfaces "adjust" to each other due to wear, relaxation, and other process, so the friction and wear decrease. This is perhaps the simplest model example of frictional self-organization, which also shows why the system that underwent the transition to a self-organized state has lower friction and wear rate. In this case the self-organization occurs due to the coupling of friction and wear [15].

The coupling of friction and elasticity can lead to the formation of a set of slip pulses, as shown in Fig. 2.6, which results in the effective decrease of the apparent coefficient of friction discussed above.

A different type of self-organization arises from coupling friction with a tribochemical reaction at the interface and formation of in situ protective tribofilms. For example, in a bronze–steel lubricated frictional system, a protective copper or lead film can form, which reduces the wear to very small values. The copper film is formed due to the anodic dissolution of bronze (an alloy of copper and tin with

additive elements). The additives, such as iron, zinc, lead, and aluminum, as well as tin, dissolved in the lubricant, while copper forms a film on the surfaces of the contacting materials. The film is in a dynamic equilibrium, while contacting layers are worn and destroyed, new layers of copper or lead are formed, resulting in virtual absence of wear and the friction force reduction by an order of magnitude. A similar effect can be achieved by the diffusion of copper ion dissolved in a lubricant. A protective layer can be formed also due to a chemical reaction of oxidation or a reaction with water vapor. For example, a self-lubricating layer of the boric acid (H_3BO_3) is formed as a result of a reaction of water molecules with B_2O_3 coating.

In general, the self-organization during friction leads in the formation of self-organized structures that result in the decrease of friction and wear and thus can be beneficial to applications. Various criteria of whether self-organization can occur in a particular tribo-system have been suggested in the literature [16–23].

2.2 Empirical Laws of Friction

In literature, a study of friction by Themistius (317–390 CE) has been regarded as the oldest ever attempt to understand friction. He found that the friction for sliding is greater than that for rolling. A more systematic experimental investigation of friction was conducted by Leonardo da Vinci in the 1500s and later by Amontons in 1699, verified by Euler in 1750 and Coulomb in 1781; are the other empirical laws of friction. They are presented as follows.

1. The friction force is directly proportional to the normal load.
2. The friction force is independent of the apparent area of contact.
3. The friction force is almost independent of the sliding velocity. Once sliding is established, the coefficient of dynamic friction is found for many systems to be nearly independent of siding velocity over quite a wide range, although at high sliding speeds, of the order of tens or hundreds of meters per second for metals.

To explain these empirical laws, it is usually assumed that (1) the friction force is proportional to the real area of contact, A, and (2) the real area of contact is proportional to the normal load, W. Thus, the friction force depends upon the real area of contact, and thus it is independent of the apparent area of contact (A_a), and the friction force is proportional to the normal load. In other words, these three rules state that the ratio of the friction force to the normal load, also called the coefficient of kinetic friction, $\mu = F/W$, is a constant, which does not change with changing W, A_a, and V, i.e., independent of W, A_a, and V [12].

The first and second Amontons–Coulomb's rules are related to each other. To illustrate, let us consider an apparent area of contact A_a which supports a normal load W, resulting in the friction force $F = \mu W$. A part of the apparent area of contact A_a/c supports the normal load W/c resulting in the friction force $F/c = \mu W/c$, where c is a constant. Let us now increase the normal load from W to cW. According to the first Amontons–Coulomb's rule, which states that F is proportional to W, such an

increase results in the friction force F and normal load W acting upon the part of apparent area of contact A_a/c. In other words, both for the whole apparent area of contact A_a and for its fraction A_a/c, the same friction force F corresponds to the load W. Thus, using only the first Amontons–Coulomb's law, it was shown that the ratio F/W is independent of the apparent area of contact, which constitutes the second Amontons–Coulomb's rule. Therefore, the load dependence of friction is coupled with its dependence on the apparent area or size of contact. In the case the load independence is violated (i.e., the μ is dependent on load), the size independence will be violated too (i.e., the μ will depend on the apparent area of contact) [12].

It is emphasized that the Amontons–Coulomb's empirical laws of friction are not fundamental laws of nature and they are not satisfied in many cases, especially at micro-/nanoscale. It is known from experiments that friction is size dependent and the coefficient of friction at micro-/nanoscale is different from that at the macroscale; load and velocity dependence of the coefficient of friction is also well established [24, 25]. Several approaches have been suggested to deal with the laws of friction at micro-/nanoscale, which include formulation of "scaling laws of friction" [24, 26–28] as well as specific nanofriction laws, which should substitute for the Amontons–Coulomb's laws at the nanoscale [25, 28].

Despite the fact that Amontons–Coulomb's laws are only approximations, they have striking universality. Equation (2.1) is valid for a very diverse range of material combinations including such classes of materials as metals, polymers, ceramics, composites, and virtually any other materials. It is also valid for normal loads ranging from nano-Newtons (in many nano-tribological applications) to thousands of tons (in geophysical applications). Furthermore, friction is a complex phenomenon that involves various apparently unrelated physical mechanisms, such as the van der Waals, covalent, and capillary adhesion, elastic and plastic deformation, brittle fracture, the so-called ratchet, cobblestone, and "third-body" mechanisms.

One way to formally explain the universality of the linear friction law is to view it as a limiting case of the viscous friction law. The viscous friction law states that the friction force is linearly proportional to the sliding velocity, and it is similar to other linear empirical laws of physics, such as the Ohm's law of electrical conductivity, the Fourier law of heat conduction, or Fick's law of diffusion. These laws describe nonequilibrium thermodynamic processes and are viewed as a consequence of nonequilibrium thermodynamic linear Onsager relationships between the so-called generalized thermodynamic forces and flows [29]. Taking into consideration the normal degree of freedom, the Onsager relationships state the linear proportionality of the velocity and forces

$$\begin{aligned} \dot{x} &= L_{11}F + L_{12}W \\ \dot{y} &= L_{21}F + L_{22}W \end{aligned} \tag{2.6}$$

where L_{ij} are the Onsager coefficients. The interface between sliding bodies has highly anisotropic properties, because a small force in the direction of the interface causes

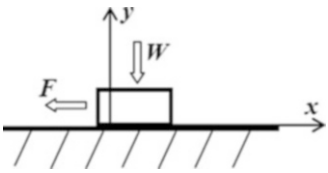

Fig. 2.8 The normal degree of freedom, y, in dynamic friction

large displacements, whereas a small force in the normal direction causes only small displacements (Fig. 2.8). To compensate for this anisotropy, we substitute coordinates using a small parameter ε as $(x,y) \rightarrow (\varepsilon x,y)$. This yields $\dot{x} = (L_{11}F + L_{12}W)/\varepsilon$, and, in the limit of $\varepsilon \rightarrow 0$, any velocity $\dot{x}$ satisfies (2.6), provided $L_{11}F + L_{12}W = 0$, which is exactly the case of Coulomb friction if $\mu = -L_{12}/L_{11}$ [29].

2.3 Friction Mechanisms

Bowden and Tabor [30] established the friction theory to explain causes of friction. According to this theory, friction has two components, namely, (a) adhesive component (μ_a) and (b) plowing component (μ_p). These components are independent to each other, such that

$$\mu = \mu_a + \mu_p \tag{2.7}$$

μ_a depends on the material pair, lubrication, and also on the real area of contact, while μ_p depends on the degree of plastic deformation taking place at the asperity level.

2.3.1 Adhesive Component

In this case contacts between two clean metal surfaces were considered. When metal surfaces are loaded against each other, they make contact only at the tips of the asperities. As the real area of contact is small, the pressure over the contacting asperities is assumed high enough to cause them to deform plastically. This plastic flow of the contacts causes an increase in the real area of contact until the real area of contact is just sufficient to support the load.

The normal force which is balanced by real area of contact is given by

$$W = AH \tag{2.8}$$

where A is the real area of contact, H is the hardness of the softer materials, and W is the normal load.

Depending on the degree of interpenetration of asperities and the surface energy, adhesive bonding occurs at the real area of contact of asperities. When these two surfaces move relative to each other, a lateral force is required to shear the adhesive

bonds formed at the interface in the regions of real area of contact. The friction force depends on the surface shear strength of the materials. The mean shear strength of the weakest junctions at real area of contact is denoted as S. Neglecting the effect of junction growth, the frictional force is given by

$$F = AS \tag{2.9}$$

$$F = \frac{W}{H}S \tag{2.10}$$

$$\frac{F}{W} = \frac{S}{H} \tag{2.11}$$

Therefore,

$$\mu = \frac{F}{W} = \frac{S}{H} \tag{2.12}$$

Thus, if adhesive component dominates frictional behavior, the friction coefficient is calculated from the ratio of shear strength of interface and hardness of soft material.

For most metals

$$S \approx \frac{H}{5} \tag{2.13}$$

Thus, in general, the adhesion theory predicts that $\mu = 0.2$, when the material pairs are similar. It should be true for any combination of the same material. But it is not true usually because of junction growth and work hardening.

2.3.2 Plowing Component

Plowing action occurs when asperities of a hard metal penetrate into a softer metal and plow out a groove by plastic deformation in the softer material. This is a major component of friction during abrasion processes, and this is probably an important factor when adhesion component is small.

Consider a harder material slides over a softer material. The harder surface was assumed to consist of large number of similar conical asperities of semi-angle θ in contact with a softer material whose surface is comparatively flat. During sliding the front surface of each conical asperity is in contact with the opposing material as shown in Fig. 2.9. Thus, the vertically projected area of contact is given by

$$A = \frac{1}{2}n\pi r^2 \tag{2.14}$$

where n is the total number of asperities.

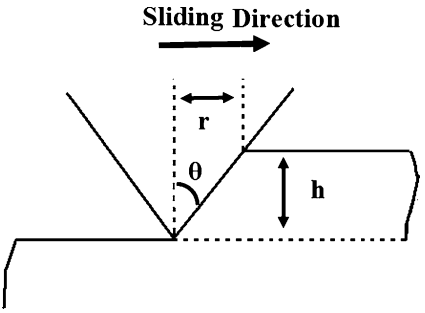

Fig. 2.9 Schematic diagram shows the plowing of a soft surface by a hard conical asperity

We know that $W = AH$; therefore,

$$W = \frac{1}{2} n\pi r^2 H \tag{2.15}$$

The friction force F is obtained in a similar manner by considering the total projected area of material, which is being displaced by plastic deformation, that is,

$$F = nrhH \tag{2.16}$$

Therefore,

$$\mu = \frac{F}{W} = \frac{2h}{\pi r} \tag{2.17}$$

However,

$$\frac{h}{r} = \cot\theta \tag{2.18}$$

Therefore,

$$\mu = \frac{2}{\pi} \cot\theta \tag{2.19}$$

2.3.3 Rolling Friction

Rolling friction is the resistance to motion that takes place when a surface is rolled over another surface. The coefficient of rolling friction between a cylindrical or spherical body against itself and a flat body generally is in the range of 5×10^{-3} to 10^{-5}. In comparison, the coefficient of sliding friction ranges typically from 0.1 to 1.

Rolling friction is not as straightforward as sliding friction. But still, there is a relationship between the rolling friction and the normal force, similar to that in sliding friction. It can be stated as

$$F_R = \mu_R W \tag{2.20}$$

where F_R is the resistive force of rolling friction, μ_R is the coefficient of rolling friction for the two surfaces, W is the normal force.

The force of rolling resistance can also be calculated by

$$F_R = \frac{(\mu_R W)}{r} \tag{2.21}$$

where F_R is the resistive force of rolling friction, r is the wheel radius, μ_R is the coefficient of rolling friction, and W is the normal force.

2.3.4 Ratchet Mechanisms

Interlocking of asperities may result in one asperity climbing upon the other, leading to the so-called ratchet mechanism. In this case, in order to maintain sliding, a driving force should be applied which is proportional to the slope of the asperity. At the atomic scale, a similar situation exists when an asperity slides upon a molecularly smooth surface and passes through the tops of molecules and valleys between them. This sliding mechanism is called "cobblestone mechanism." This mechanism implies that the strong bonds are acting in the bulk of the body, whereas interface bonds are weak.

2.3.5 Brittle Fracture and Plastic Inception Mechanisms

For a brittle material, asperities can break forming wear debris. Therefore, fracture also can contribute to friction. There is also an analogy between mode II crack propagation and sliding of an asperity [31–33]. When an asperity slides, the bonds are breaking at the rear, while new bonds are being created at the front end. Thus, the rear edge of an asperity can be viewed as a tip of a propagating mode II crack, while the front edge can be viewed as a closing crack. Gliding dislocations, emitted from the crack tip, can also lead to the microslip or local relative motion of the two bodies [24]. Calculations have been conducted to relate the stress intensity factors with friction parameters [31–33]. Crack and dislocation propagation along the interface implies that the interface is weak compared to the bulk of the body.

Chang et al. [34] proposed a model of friction based upon plastic yield, which was later modified by Kogut and Etzion [35]. They considered a single-asperity contact of a rigid asperity with an elastic–plastic material. With an increasing normal load, the maximum shear strength grows and the onset of yielding is possible. The maximum shear strength occurs at a certain depth in the bulk of the body. When the load is further increased and the tangential load is applied, the plastic zone grows and reaches the interface. This corresponds to the onset of sliding. Kogut and Etzion [35] calculated the tangential load at the onset of sliding as a function of the normal load using the finite elements analysis and found a nonlinear dependence between the shear and tangential forces. This mechanism involves plasticity and implies structural vulnerability of the interface compared to the bulk of the contacting bodies.

2.3.6 The "Third-Body" Mechanism

During the contact of two solid bodies, wear and contamination particles can be trapped at the interface between the bodies. Along with liquid which condensates at the interface, they form the so-called third body which plays a significant role in friction. The trapped particles can significantly increase the coefficient of friction due to plowing. Some particles can also roll and thus serve as rolling bearings, leading to reduced coefficient of friction. However, in most engineering situations, only 10 % of the particles roll and thus the third-body mechanism leads to an increase of the coefficient of friction. At the atomic scale, adsorbed mobile molecules can constitute the "third body" and lead to significant friction increase [36]. The third body has much weaker bonds to the surface, than those in the bulk of the body.

2.3.7 Effect of Surface Roughness

Various statistical models of contacting rough surfaces have been proposed following the pioneering work by Greenwood and Williamson [37] that considered a random distribution of asperity heights. These models conclude, using the numerical computations, that for typical roughness height distributions (such as the Gaussian roughness) for both elastic and plastic materials, the real area of contact is almost linearly proportional to the load [7]. For the elastic contact of a smooth surface and a rough surface with the correlation length β^* and standard deviation of profile height σ, the real area of contact is given by

$$A_r \propto \frac{\beta^*}{E^*\sigma} W \tag{2.22}$$

where E^* is the composite elastic modulus of the two bodies [3]. Note that σ is the vertical and β^* is the horizontal roughness parameters with the dimension of length. The smoother the surface (the higher the ratio β^*/σ), the larger the A_r is. Physically, the almost linear dependence of the real area of contact upon the normal load in this case is a result of the small extent of contact; in other words, it is the consequence of the fact that the real area of contact is a small fraction of the nominal area of contact. With increasing load, as the fraction of the real area of contact grows, or for very elastic materials, such as the rubber, the dependence is significantly nonlinear. However, for small real area of contact, with increasing load the area of contact for every individual asperity grows, but the number of asperity contacts also grows, so the average contact area per asperity remains almost constant.

For plastic contact, the real area of contact is independent of roughness parameters and given by the ratio of the normal load to the hardness of a softer material H [3]

$$A_r = \frac{W}{H} \tag{2.23}$$

Hardness is usually defined in indentation experiments as force divided by the indentation area, so (2.23) naturally follows from this definition. In many cases it may be assumed that the hardness is proportional to the yield strength. Whether the contact is elastic or plastic may depend upon the roughness parameters, elastic modulus, and hardness. Interestingly, Greenwood and Williamson [37] showed whether the contact is elastic or plastic does not depend upon the load, but solely upon the so-called plasticity index $\psi = \left(\sqrt{\sigma/R_p}\right)E^*/H$, where σ is the standard deviation of peak heights and R_p is the mean asperity peak radius.

Fractal models provide an alternative description of a rough surface. Long before the discovery of fractals by mathematicians, Archard [38] studied multi-scale roughness with small asperities on top of bigger asperities, with even smaller asperities on top of those, and so on. According to the Hertzian model, for the contact of an elastic sphere of radius R loaded against an elastic flat with the contact radius a, the contact area $A = \pi a^2$ are related the normal load as

$$A_r = \pi\left(\frac{3RW}{4E^*}\right)^{2/3} \tag{2.24}$$

The pressure distribution as the function of the distance from the center of the contact spot, r, is given by

$$p = \left(\frac{6WE^{*2}}{\pi^3 R^2}\right)^{1/3}\sqrt{1-(r/a)^2} \tag{2.25}$$

Let us now assume that the big spherical asperity is covered uniformly by many asperities with a much smaller radius, and these asperities form the contact. For an asperity located at the distance r from the center, the load is proportional to the stress given by (2.25). The area of contact of this small asperity is still given by (2.24) with using the corresponding load. The dependence of total contact area upon W is then given by the integration of the individual contact areas by r as [38]

$$\begin{aligned} A_r &\propto \int_0^a \left[W^{(1/3)}\sqrt{1-r^2/a^2}\right]^{2/3} 2\pi r dr \\ &\propto \int_0^\pi \left[W^{(1/3)}\cos\phi\right]^{2/3} 2\pi(a\sin\phi)a\cos\phi d\phi \\ &\propto W^{(2/9)}a^2 \propto W^{(2/9)}W^{(2/3)} \propto W^{(8/9)} \end{aligned} \tag{2.26}$$

In the above derivation, the variable change $r = a\sin\phi$. The integral of the trigonometric functions can be easily calculated; however, its value is not important for us, because it is independent of a and W.

If the small asperities are covered by the "third-order" asperities of even smaller radius, the total area of contact can be calculated in a similar way as

$$A_r \propto \int_0^a \left[W^{(1/3)}\sqrt{1-r^2/a^2}\right]^{8/9} 2\pi r dr \propto W^{(8/27)}a^2 \propto W^{(26/27)} \tag{2.27}$$

For elastic contact, it is found

$$A_r \propto W^{\frac{3^n-1}{3^n}} \tag{2.28}$$

where n is the number of orders of asperities, leading to an almost linear dependence of A_r upon W with increasing n. Later more sophisticated fractal surface models were introduced, which lead to similar results.

Thus both statistical and fractal roughness, for elastic and plastic contact, combined with the adhesive friction law results in an almost linear dependence of the friction force upon the normal load.

2.4 Factors Affecting Friction

Surface roughness: One of the early attempts to explain friction was to relate it to surface roughness because surface is not generally smooth; instead it consists of asperities (i.e., short-range perturbations from the mean) and waviness (i.e., long-range perturbations from the mean). The roughness theory assumed that the frictional force is equal to the force required to climb up the asperity of slope θ and the coefficient of friction was described as a function of tan θ [39]. However, it is clear that asperities undergo deformation due to the sliding action rather than simply sliding over each other. In very smooth surfaces, the real area of contact grows rapidly, and so is the friction, whereas with very rough surfaces the friction is high again because of the need to lift one surface over the asperities on the other. In the intermediate range of roughness that normally used in engineering practice, the friction is at minimum and almost independent of the roughness [40].

Surface topography: The influence of the surface topography on friction reduction is not well established. Early research in this direction focused on aspects such as the real area of contact and the lubricant trapping and tried to highlight the significance of surface topography [41]. Later on the effect of surface topography on friction was studied in detail [42–52]. Several well-known roughness parameters were used to quantify surface topography [53–62]. Surface roughness parameter such as the average roughness, R_a, is used to describe a surface topography. However, such a single roughness parameter cannot describe a functional characteristic like friction, and it is possible that two surface topographies can have the same R_a, but their frictional characteristics could be significantly different [63–65]. Attempts were made to correlate surface roughness parameters with friction [66–68]. In addition, new roughness parameters were formulated to correlate with friction [61, 69–71]. In general, the correlation coefficient between the coefficient of friction and the roughness parameters was system dependent.

Crystal structure: Effect of material crystal structure on friction depends on how easily material can undergo plastic deformation. Ease of plastic deformation of a material depends on the number of slip systems available. It is well known that a

minimum of five independent slip systems are required for plastic deformation to take place by slip. Hexagonal metals have a limited number of slip systems, and thus the chance for forming higher real area of contact is less due to lack of plastic deformation when compared with FCC metals. Hence, HCP metals experience lower friction coefficients than FCC and BCC metals in which a larger number of slip systems are available for plastic deformation [72–76]. Since crystal structures affect friction, it could be expected that allotropic metals exhibit a similar influence on either side of a transition temperature due to phase transformation. Further, the lattice parameters in HCP metals influence the number of operating slip systems and thus more easily undergo plastic deformation which in turn influences the friction. HCP metals with close to ideal atomic stacking ratio (c/a = 1.633), e.g., Co, Rh, and Mg, primarily slip along basal planes and have low friction coefficients. Metals which deviate considerably from ideal stacking such as titanium (c/a = 1.587) will exhibit primarily non-basal slip mechanisms and higher friction coefficients.

Strain hardening and hardness: It is well established that severe plastic deformation occurs in the surface regions (e.g., asperity contacts) of a metal sliding over a harder surface. This results in the surface of the metal being progressively work hardened, and the surface will reach a maximum hardness that depends on the method by which it has been deformed [77, 78]. In general, coefficient of friction is an inverse function of hardness of a metal. The effect of hardness on friction is attributed to the fact that lack of plastic deformability of hard metals, with subsequent decrease in the ability of metals to adhere, results in low friction [71, 79, 80]. The atomic bonds in harder metals are strong and hence the resistance to adhesion is increased, providing low frictional characteristics. However, coefficient of friction is not necessarily lower for harder materials; hardness alone cannot be used as a criterion for predicting the coefficient of friction [81].

Elastic and shear modulus: Any increase in elastic modulus results in a decrease in real area of contact and thus reduces the adhesion and friction. The shear modulus, behaves like the elastic modulus because it relates by E = 2.6 G, affects the frictional behavior of metals. Thus, the friction coefficient decreases with an increase in shear modulus [82].

Grain size: Effects of grain size on frictional characteristics of many materials have been studied in combination with their wear behavior. It was stated that friction coefficient decreases with a decrease in grain size [83–86]. One of the important consequences of this is the improved mechanical and chemical properties of nanocrystalline materials. Thus, nanocrystalline materials are of great industrial importance, and their wide spread use in modern technology is quite evident in areas such as MEMS. These materials are used as bulk as well as coatings to engineering substrates.

Surface energy: In dry clean conditions, adhesion and friction strongly depend upon the surface energy of the materials [40]. Metals which have high surface energies form adsorbed layers by reacting with gaseous and liquid molecules in air.

The existence of adsorbed layer reduces surface energy of metals and also decreases the friction coefficient. When there is no gaseous environment, higher values of the ratio of surface energy to hardness of metals correspond to large adhesion and a high friction coefficient.

Normal load: Some metals (e.g., Cu, Al) which oxidize in air show lower friction at low loads as a result of oxide film formation that effectively separates the two metal surfaces and exhibits high friction at high loads due to breakdown of the oxide film [87].

Sliding velocity: High sliding velocities result in surface frictional heating and thus formation of a thin molten layer at the asperity contacts which reduces the shear strength at the contact resulting in very low friction coefficient. This thin molten film acts as lubricant between sliding surfaces [88]. Generally, the friction coefficient decreases with an increase in sliding velocity. Formation of oxide layers on metal surfaces at high temperature, which is induced by sliding speed, results in low friction. On the other hand, softening of the metal surface may result in high friction due to increased plowing in the softer material. Both of these two factors make it difficult to predict the effect of sliding velocity on friction.

Environment: In ambient conditions, most metals oxidize and form oxide films, typically between 1 and 10 nm thick within a few minutes of exposure of clean surfaces. This oxide films act as low shear strength film and minimize the metal–metal contact at asperity level and thus lead to low friction. On the other hand, in vacuum condition, there is less chance of oxidation and direct contact existing between metal–metal surfaces. In this case, depending on metallurgical compatibility, the level of adhesion governs the frictional behavior of the metals. The values of the friction coefficient in vacuum were about 10 times higher than values measured in air [89].

Temperature: An increase in the temperature generally results in metal softening. When the temperature of a sliding metal is increased, several effects occur. The mechanical properties of the contacting metals will change, the rate of oxidation will increase, and a phase transformation may take place. All these factors will influence the frictional behavior.

2.5 Friction of Materials

The coefficient of friction depends on the experimental conditions under which it is measured [90]. In general, clean metal surfaces under vacuum show strong adhesion and high coefficient of friction, typically 2–10. Strong metallic bonds are formed across the interface in high vacuum. However, in most practical application, metals slide against one another in air, and the coefficient of friction values are much lower than in vacuum and lie typically for dry sliding, in the range from 0.2 to 1.0. Some metals oxidize in air to form oxide films that are typically between 1 and

10 nm thick within a few minutes of exposure. The oxide film acts as a low shear strength film and also due to low ductility of the film leads to low friction. The oxide film may effectively separate the two metallic surfaces. The friction between oxide surfaces or between oxide and bare metal surfaces is almost always less than between surfaces of bare metals. At low normal loads, the oxide films effectively separate the two metal surfaces, and there is little or no true metallic contact. Thus, the coefficient of friction is low. As the normal load is increased, a transition occurs to a higher value of the coefficient of friction. This could be due to the breakdown of oxide films due to higher loads imposed during sliding. Hexagonal metals such as Mg, Zn, and Co exhibit low friction. In general, the coefficient of friction for an alloy tends to be rather less than that for its pure components [91].

Ceramics exhibit high mechanical strength, do not lose their strength or oxidize readily at elevated temperatures, and are resistant to corrosive environments. Ceramic materials are much less ductile than metals. The mechanical behavior of ceramics differs from that of metals or alloys due to the different nature of the interatomic forces with covalent or ionic bonding in ceramics compared to that of metallic bonding in metals or alloys. The nature of contact between ceramics is more likely to be elastic than in metals. Although adhesive forces (due to covalent, ionic, or van der Waals bonds) are present between ceramic materials in contact, low real area of contact results in relatively low values of coefficient of friction comparable to metallic couples. The coefficient of friction of ceramic pairs does not reach as high values as that of metals under similar testing conditions. The coefficient of friction value for ceramic–ceramic contacts lies typically in the range from 0.2 to 0.8. These are similar to the values seen for metallic couples sliding in air in the presence of intact oxide films, and indeed, there is much similarity between the contact of oxidized metal surfaces and that of bulk oxide ceramics.

Polymers are more compliant than metals or ceramics with elastic modulus values typically one-tenth or even less. Their strength is also much lower. They are often used in sliding applications against hard mating surfaces. In polymers, the contact between polymers or between a polymer and a metal is often predominantly elastic and creates transfer layers. In this respect, the friction of polymers differs fundamentally from that of metals. Coefficient of friction between polymers sliding against themselves or against metals or ceramics commonly lies in the range from 0.1 to 0.5. The friction of polymers, like that of metals, can be attributed to two sources, namely, adhesion and plowing. Many polymers sliding against hard counterfaces (e.g., metals) transfer detectable films of polymers onto the counterface [60, 92, 93]. The formation and behavior of the transfer films are important factors in the friction and wear of these polymers.

2.6 Friction Measurement Devices

Any apparatus for measuring friction must be capable of supplying relative motion between two specimens, of applying a measurable normal load, and of measuring the tangential resistance to motion. Many accelerated test apparatuses are commercially

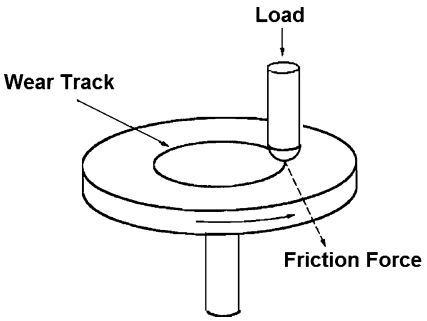

Fig. 2.10 Schematic of pin-on-disk test system

available that allow control of such variables like sample geometry, load, velocity, temperature, and environment. The most commonly used device is a pin-on-disk apparatus. As shown in Fig. 2.10, the disk is driven continuously while the pin is normally stationary with a load applied to it. In the pin-on-disk apparatus, the pin is held stationary and the disk rotates. The pin can be a nonrotating ball (ball-on-disk configuration), a hemispherically tipped rider, or a flat-ended cylinder.

2.6.1 Other Important Apparatus

Pin-on-flat: In the pin-on-flat apparatus, a flat moves relative to a stationary pin in reciprocating motion. In some cases, the flat is stationary and the pin reciprocates. The pin can be a ball, a hemispherically tipped pin, or a flat-ended cylinder.

Pin-on-cylinder: The pin-on-cylinder apparatus is similar to the pin-on-disk apparatus, except that loading of the pin is perpendicular to the axis of rotation. The pin can be flat or hemispherically tipped.

Flats-on-rotating-cylinder: In the flats-on-rotating-cylinder apparatus, two rectangular flats are loaded perpendicular to the axis of rotation of the disk.

Crossed-cylinder: The crossed-cylinder apparatus consists of a stationary solid cylinder and a rotating solid cylinder that operates perpendicular to the stationary cylinder.

Four-ball: The four-ball apparatus consists of four balls in the configuration of an equilateral tetrahedron. The upper ball rotates and rubs against the lower three balls which are held in a fixed position.

3 Wear

Wear is the progressive loss of substance from the surface of a body brought about by mechanical action. In most cases, wear occurs due to surface interactions at the asperities. During relative motion, material on the contact surface may be displaced

Table 2.1 Different types of wear mechanisms, definitions, and characteristics

Mechanisms	Definitions	Characteristics
Adhesion	Wear due to transfer of material from one surface to another surface by shearing of solid welded junctions of asperities	Adhesive bonding, shearing, and material transfer
Abrasion	Wear due to hard particles or protuberances sliding along a soft solid surface	Plowing, wedging, and cutting
Delamination	Wear caused by delamination of thin material sheets beneath the interface in the subsurface	Plastic deformation, crack nucleation, and propagation
Erosion	Wear due to mechanical interaction between solid surface and a fluid, or impinging liquid or solid particles	Angle of incidence, large-scale subsurface deformation, crack initiation, and propagation
Fretting	Wear due to small amplitude oscillatory tangential movement between two surfaces	Relative displacement amplitude and entrapment of wear particles
Fatigue	Wear caused by fracture arising from surface fatigue	Cyclic loading and fatigue crack propagation
Corrosive/oxidative wear	Wear occurs when sliding takes place in corrosive/oxidative environment	Formation of weak, mechanically incompatible corrosive/oxide layer

so that properties of the solid body near the surface are altered; then material may be removed from a surface and may result in the transfer to the mating surface or may break lose as a wear particle. Wear, as friction, is not a material property; it is a system response. Operating conditions affect the wear process. Sometimes it is assumed that high friction correlates to a high wear rate. This is necessarily not true. Wear is quantified by the term "wear rate" which is defined as the mass or volume or height loss of material removed per unit time or sliding distance.

3.1 Wear Mechanisms

The important wear mechanisms are adhesive wear, abrasive wear, delamination wear, erosive wear, fretting wear, fatigue wear, and corrosive/oxidative wear. The characteristic features and definitions of different wear mechanisms are given in Table 2.1. In general, two-thirds of all wear processes encountered in industrial situations occurs due to adhesive and abrasive wear mechanisms. In many cases, wear is initiated by one mechanism, and it may proceed by other wear mechanisms. Wear components are generally examined to determine the type of wear mechanism by using microscopy or surface analytical techniques.

Wear is also expressed based on scale size of wear debris such as mild wear and severe wear. In mild wear, wear occurs at the outer surface layers and worn

debris contains fine oxide particles of size that varies from 0.01 to 100 nm. In severe wear, wear occurs at deep surfaces and size of wear debris ranges from 100 nm to 100 μm.

3.1.1 Adhesive Wear

When two atomically clean solid surfaces are brought together, the atoms must be in contact at some points. Thus, two surfaces will experience short-range van der Waals forces. At distance of about 1 nm, strong short-range forces come into action, and strong adhesive junctions may be formed at the real area of contact. When there is relative motion, the adhered junctions are sheared. The net result is that softer material is transferred to harder surface. Soft material may adhere to hard surface, or on the other hand, subsequent sliding produces a loose wear debris. The amount of wear depends on the location at the junctions that is sheared. More specifically, if shear takes place at the original interface, then the wear is zero. However, if shear takes place away from the interface, a fragment of material is transferred from one surface to the other. In practice, the transfer of material is observed from the softer material to the harder material, but occasionally from the harder material to the softer material. Adhesive wear is often called galling, scuffing, cold welding, or smearing.

Archard [94] derived a theoretical expression for the rate of adhesive wear. In this theory, it was assumed that the area of contact comprises a number of circular contact spots, each of radius a. Then the area of each contact spot is πa^2.

Each contact supports a normal load

$$W = \pi a^2 H \tag{2.29}$$

where H is the hardness of the soft material.

If there are n number of contacts, then the total normal load $W = n\pi a^2 H$ or

$$n\pi a^2 = \frac{W}{H} \tag{2.30}$$

During sliding, the opposing surface will pass over the asperity for a sliding distance $2a$.

It is assumed that the wear fragment produced from each asperity is hemispherical in shape and of volume

$$v = \frac{2}{3}\pi a^3 \tag{2.31}$$

Then the wear volume δQ produced by one asperity contact in unit sliding distance is given by

$$\delta Q = \frac{\frac{2}{3}\pi a^3}{2a} = \frac{\pi a^2}{3} \tag{2.32}$$

The total wear volume Q per unit sliding distance is

$$Q = \frac{n\pi a^2}{3} \tag{2.33}$$

where n is the total number of contacts.

Substituting (2.30) in (2.33), we get

$$Q = \frac{W}{3H} \tag{2.34}$$

This equation suggests that:

(a) Wear volume is proportional to the load.
(b) Wear volume is inversely proportional to the hardness of the softer material.
(c) Wear volume is proportional to the sliding distance.

In general, the experimental results proved that the wear volume is much less than the theoretical predictions by several orders of magnitude. Equation (2.34) was derived by assuming that a wear particle was produced at each asperity encounter. Thus, this theory is modified by considering the experimental results and postulating that wear particles produced only a fraction k of such encounter, so that

$$Q = k\frac{W}{3H} \tag{2.35}$$

Or $Q = K\frac{W}{H}$ or for "x" sliding distance

$$Q = K\frac{Wx}{H} \tag{2.36}$$

where $K = \frac{k}{3}$ and is called wear coefficient.

Thus, the uncertainty in predicting a wear rate is due to the uncertainty in the value of K, and this must be found experimentally for different combination of sliding materials and different conditions of rubbing. The value of K ranges typically from 10^{-8} to 10^{-4} for mild wear and from 10^{-4} to 10^{-2} for severe wear for most material combinations, depending on the operating conditions.

3.1.2 Abrasive Wear

Consider a situation in which a hard material is kept in contact with the soft solid surface. The asperities of hard materials are pressed into the soft surface with plastic flow of the soft surface. When tangential movement is imposed, the hard material will slide and remove the soft material by plowing. Thus, the abrasion process includes several deformation modes such as plowing, wedge formation, and cutting. Plowing causes a series of grooves as a result of plastic flow of the softer material.

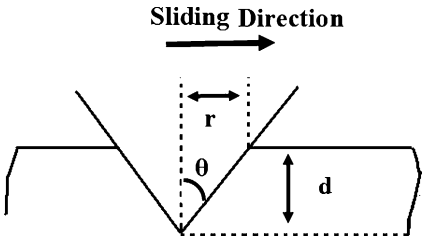

Fig. 2.11 Abrasive wear by conical asperity

In wedge formation, an abrasive tip plows a groove and develops a wedge on its front. In cutting form, an abrasive tip cuts a groove and removes the material. Abrasion is typically categorized according to type of contact as two-body and three-body abrasion. In two-body abrasion, a hard material slides along a soft surface. In three-body abrasion, wear debris are caught between two surfaces and cause one or both of them to be abraded. Wear loss in a two-body abrasion is typically 10–1,000 times greater than three-body abrasion for given load and sliding distance.

The well-known model of abrasive wear assumes that the abrasive asperity is like a sharp tool which has a conical shape, defined by the angle θ, plowing a track through the softer flat surface and removes a material as shown in Fig. 2.11. In traversing unit distance, it displaces a volume of material

$$v = rd \tag{2.37}$$

It can be seen from Fig. 2.11 that

$$d = r \tan \theta \tag{2.38}$$

Therefore,

$$v = r^2 \tan \theta \tag{2.39}$$

The total volume of material displaced in unit sliding distance

$$Q = nr^2 \tan \theta \tag{2.40}$$

where n is the number of asperity contacts.

For simplicity, we assume that the softer material has yielded due to normal load alone. Therefore, the abrasive wear particle transmits a normal load of

$$W = \pi r^2 \frac{H}{2} \tag{2.41}$$

where H is the hardness of the softer material.

Thus, if there are n asperity contacts, the normal load

$$W = n\pi r^2 \frac{H}{2} \tag{2.42}$$

or

$$nr^2 = \frac{2}{\pi}\frac{W}{H} \tag{2.43}$$

Substituting (2.43) in (2.40), we get

$$Q = \frac{2}{\pi}\frac{W}{H}\tan\theta \tag{2.44}$$

Similar to adhesive wear, it is found that not all abrasive particles produce loose wear debris.

Thus,

$$Q = k\frac{W}{H}\frac{\tan\theta}{\pi} \tag{2.45}$$

where k is the proportion of events that actually produces wear particles.

Or

$Q = K\frac{W}{H}$ or for "x" sliding distance

$$Q = K\frac{Wx}{H} \tag{2.46}$$

where $K = k\dfrac{\tan\theta}{\pi}$

Equation (2.46) is of the same form of as the adhesive wear (2.36), and according to this simple derivation, the laws of wear which are derived from (2.36) should apply equally well to abrasive wear.

In the above derivation we assumed that all the material displaced by the abrasive particles becomes loose wear debris. However, this is not true. Examination of abraded surfaces showed that much of the displaced material can be simply piled up at the sides of the grooves and not lost to the surface. The value of K typically ranges from 10^{-6} to 10^{-1}.

3.1.3 Delamination Wear

The delamination theory of wear was first put forward by Suh [95] to describe the wear of surfaces in sliding contact. This theory describes the production of laminate wear debris in the following way:

1. When two surfaces come in to contact, normal and tangential loads are transmitted through the contact points. The material at the surface and very near the surface does not have a high dislocation density during sliding. This is due to the

elimination of dislocations by the image force acting on those dislocations which are parallel to the surface. Therefore, cold-working of the material very near the surface is less than that at the subsurface.
2. The surface traction exerted by the harder asperities at the contact points induces incremental plastic shear deformation which accumulates with repeated loading in the subsurface. As subsurface deformation continues, there will be pileups of dislocations at finite distance from the surface. As time progresses, the piled up dislocations will lead to the formation of microvoids or cracks. Thus, cracks are nucleated below the surface.
3. As time progresses further, these cracks will coalesce, either by growth or shearing of the metal, and propagate parallel to the wear surface. The depth of crack nucleation and distance of propagation depend on material properties, normal load, and friction characteristics of the surface. When this crack reaches a critical length, the material between the crack and the surface will shear, yielding long and thin laminated wear debris.

3.1.4 Erosion Wear

Erosion is the form of damage experienced by a solid body when liquid or solid particles impinge on a solid surface. There are basically two types, namely, solid erosion and fluid erosion.

Solid erosion is a form of abrasive wear and is treated differently because the contact stress arises from the kinetic energy of particles flowing in air as it encounters the surface. The particle velocity, impact angle, and the size of the abrasive particle give a measure of the kinetic energy of the impinging particle. Wear debris are formed in erosion as a result of repeated impacts. As in the case of abrasive wear, erosive wear occurs by plastic deformation and/or brittle fracture, depending on material being eroded away and on operating conditions. Wear rate dependence on the impact angle for ductile and brittle materials is different (see Fig. 2.12). For ductile materials the maximum erosion occurs at an angle of approximately 20°. Ductile material will undergo wear by a process of plastic deformation in which the material is removed by the displacing or cutting action of the eroded particle. In brittle materials, the material is removed by the formation and intersection of cracks that radiate out from the point of impact of the eroded particle. The shape of the abrasive particles also affects the wear rate. Sharper particles would lead to more localized deformation and hence higher wear rates as compared to the rounded particles.

In fluid erosion, there are basically two types—liquid impact erosion and cavitation erosion. When tiny liquid drops strike the solid surface at high speeds, due to high pressure, materials can undergo plastic deformation or fracture, and repeated impacts lead to pitting and erosive wear. In many cases, pure liquid impingement erosion is an unlikely mechanism, and erosion–corrosion mechanism usually does more damage. In ductile materials, a single intense impact may produce a central depression with a ring of plastic deformation around it where

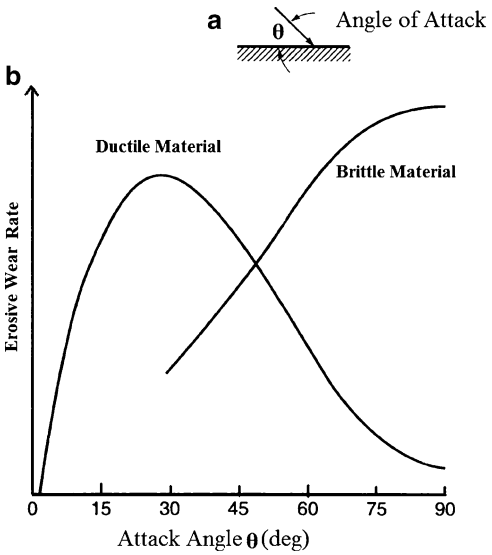

Fig. 2.12 Rate of erosive wear as a function of attaché angle of impinging particles for ductile and brittle materials

the jetting outflow may remove the material by a tearing action. In brittle materials, circumferential cracks may form around the impact site, caused by tensile stress waves propagating outward along the surface. With continued impacts, material can spall off the inside surface due to the compressive stress wave from the impact reflecting there as a tensile wave. Cavitation damage occurs when bubbles entrained in a liquid become unstable and implode against the surface of a solid. When bubbles collapse that are in contact with or very close to a solid surface, it will collapse asymmetrically, forming a micro-jet of liquid directed towards the solid. The solid material will absorb the impact energy as elastic deformation, plastic deformation, or fracture. The latter two processes may cause localized deformation and/or erosion of the solid surface.

3.1.5 Fatigue Wear

Fatigue wear can be an important phenomenon on two scales: macroscopic and microscopic. Macroscopic fatigue occurs at nonconforming loaded surfaces, such as those found in rolling contacts, whereas microscopic fatigue occurs at the contacts between sliding asperities. In other words, subsurface fatigue and surface fatigue are observed during repeated rolling and sliding, respectively. The repeated loading and unloading cycles may induce the formation of subsurface or surface cracks. Eventually, after a critical number of cycles, these cracks will result in the breakup of the surface with the formation of large fragments, leaving large pits in the surface, also known as pitting. Prior to the critical number of cycles, negligible wear takes place, which is in contrast to the wear caused by an adhesive or abrasive mechanism, where wear causes a gradual deterioration from the start of running.

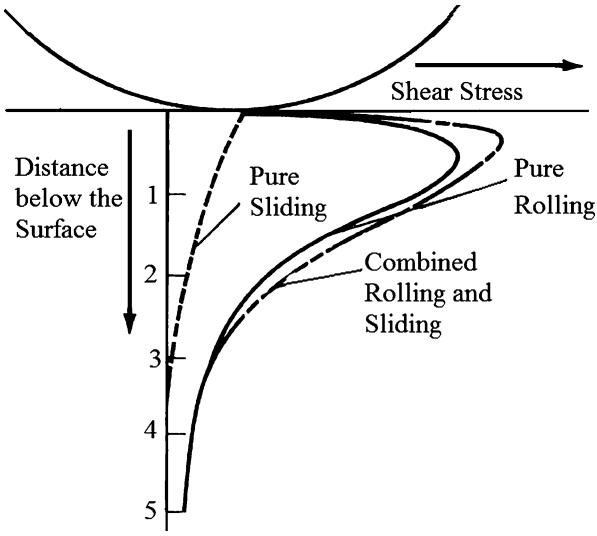

Fig. 2.13 Variation of principal shear stress at various depths directly below the point of contact of two hard surfaces in pure rolling, pure sliding, and a combination contact. The "z" is the distance below the surface in the vertical direction and "a" is half of the Hertzian diameter

Rolling contact fatigue: In rolling fatigue, under dry conditions, adhesive and abrasive wear mechanisms are operative during direct physical contact between two moving surfaces relative to each other. In well-lubricated rolling conditions, these wear mechanisms do not operate and there is no progressive visible wear. However, the life of rolling components is limited by the fatigue. At the rolling interface, the contact stresses are very high and fatigue mechanism can be operative. In these cases, although direct solid–solid contact does not occur, the mating surfaces experience large stresses which are transmitted through the lubricating film during the rolling motion. In the presence of such stresses, the maximum compressive stress occurs at the surface, but the maximum shear stress occurs at some distance below the surface (Fig. 2.13). As rolling proceeds, any subsurface element is subject to a stress cycle for each passage of a roller. Time to fatigue failure is dependent on the amplitude of the reversed shear stresses. If the stress amplitude is above the fatigue limit, fatigue failure will eventually occur. The position of failure in a perfect material subjected to pure rolling contact would be defined by the position of maximum shear stress given by the Hertz equations. In practice, materials are never perfect and the position of failure would normally depend on microstructural factors such as the presence of inclusions or microcracks. When a fatigue crack does develop, it occurs below the surface until a region of metal is separated to some extent from the base metal by the crack and ultimately becomes detached and spalls out. By the time cracks grow large enough to emerge at the surface and produce wear particles, these particles may become large flakes.

Sliding contact fatigue: When sliding surfaces make contact at the asperities, wear takes place by adhesion and abrasion. However, in sliding fatigue, asperities can make contact without adhering or abrading and can pass each other, leaving one or

both asperities plastically deformed due to contact stresses. As the surface and subsurface deformation continues, cracks nucleate at and below the surface. Once the cracks are formed, further loading and deformation causes cracks to extend and propagate. After a critical number of cyclic contacts, an asperity fails due to fatigue, producing a wear fragment. In sliding contact, friction is generally high compared to a rolling contact; the maximum shear stress occurs at the surface which leads to surface fatigue.

3.1.6 Fretting Wear

Fretting can occur whenever low-amplitude oscillatory motion in the tangential direction takes place between the contacting surfaces. This is a common occurrence in machinery which is subjected to vibration. Fretting can combine many of the wear process. Basically, fretting is a form of adhesive or abrasive wear, where the normal load causes adhesion between asperities and oscillatory movement causes rupture, resulting in wear debris. Most commonly, fretting is combined with corrosion, in which case the wear mode is known as fretting corrosion. Fretting in corrosive environment produces wear particles which are harder than their parent metals and this can lead to abrasion. The fact that there is no macroscopic sliding at fretting contacts so the fretting wear debris cannot escape easily but is trapped between the surfaces. Therefore, the amount of wear per unit sliding distance due to fretting may be larger than that of adhesive and abrasive wear. The oscillatory sliding can also cause vibration and thus chances of forming fatigue failure. This kind of failure is known as fretting fatigue.

3.1.7 Corrosive/Oxidative Wear

Corrosive wear occurs when sliding takes place in a corrosive environment. In air, the most dominant corrosive medium is oxygen. Therefore, corrosive wear in air is generally called oxidative wear. However, the same principles would apply to wear in any other type of corrosive medium. In the absence of sliding, oxide films typically less than a micrometer thick form on the surfaces. Sliding action wears the oxide film away so that corrosive attack can continue. Thus, corrosive wear requires corrosion and rubbing. Machinery operating near the coast generally produces corrosive wear more rapidly than that operating in a clean environment.

It is important to note that oxidation on the sliding surfaces is usually beneficial. Formations of oxide films act as solid lubricant and prevent metal–metal contact and thus mitigate against the severe adhesion-enhanced wear which would otherwise occur. Oxidation can reduce the wear rate of metallic pairs by two orders of magnitude, as compared with that of the same pair in an inert atmosphere. Very often, when surfaces are oxidized, the wear debris is finely divided oxide, the rubbing surfaces remain smooth, and the rate of loss of material is low. The effects of oxidation depend not only on the oxidation rate but also on the mechanical properties of both the oxide and the base metal and the adhesion of the oxide to the

base metal. Oxidation is a thermally activated process; the rate of oxidation can increase exponentially with temperature. A change of only few degrees in surface temperature can change the rate of oxidation by an order of magnitude.

3.2 Thermodynamic Models of Wear

Friction and wear are dissipative irreversible processes. Entropy is the measure of irreversibility and dissipation. Therefore, entropy can be used to characterize wear and related degradation processes. Manufacturing, which transforms nature's raw materials into highly organized finished components, reduces entropy. Aging or degradation from friction and wear tends to return these components back to natural states. Accordingly, entropy must monotonically increase to be consistent with laws of thermodynamics.

The attempts to use thermodynamic methods for a general theory of wear have been taken by many researchers; however, most of these attempts had limited success due to the complexity of the equations involved and the difficulty of their solution [96–98]. Doelling et al. [99] experimentally correlated wear with entropy flow, dS/dt, at a wearing surface and found that wear was roughly proportional to the entropy produced for the steady sliding of copper on steel under boundary lubricated conditions. Bryant et al. [100] conducted an interesting entropic study of wear. They started from the assumption that friction and wear are manifestations of the same dissipative physical processes occurring at sliding interfaces. The production of irreversible entropy by interfacial dissipative processes is associated with both friction and wear. Friction force dissipates power and generates entropy, whereas wear irreversibly changes material's structure, often with loss of material. Bryant [98] identified entropy production mechanisms during various dissipative processes relevant to friction and wear, which are summarized in Table 2.2. It is observed that the change of entropy has the general form of $dS = Y d\xi$, that is, a thermodynamic force Y times the change of the generalized coordinate $d\xi$.

The concept of entropy can be applied to friction, surface degradation, and self-organization. Manufacturing transforms raw materials into highly organized components, while aging and degradation tend to return them into their natural disordered state [100]. The entropy production rate is given by

$$\frac{dS}{dt} = XJ \tag{2.47}$$

where J is the thermodynamic flow rate and X is a generalized thermodynamic force [15].

Consider now frictional sliding with the velocity $V = dx/dt$, applied normal load W, and friction force $F = \mu W$. The work of the friction force is equal to the dissipated energy, and we will assume now that all dissipation energy is converted into the heat

Table 2.2 Entropy change during various dissipative processes (based on Bryant 98)

Process	Entropy change
Adhesion	$dS = \frac{\gamma dA}{T}$, where γ is the surface energy, A area
Plastic deformation	$dS = \frac{U_p dV}{T}$, where U_p is the work per volume, V volume
Fracture	$dS = \frac{\left(\frac{\partial U}{\partial a} - 2\gamma\right) da}{T}$, where $\frac{\partial U}{\partial a}$ is the energy release rate, a is crack length
Phase transition	$dS = \frac{dH}{T}$, where H is the enthalpy
Chemical reaction	$dS = \frac{\sum_{react} \mu_i dN_i - \sum_{products} \mu_i dN_i}{T}$, where N_i are the numbers of molecules and μ_i are the chemical potentials for reactants and products
Mixing	$\Delta S = -R\sum_{i}^{n} \frac{N_i}{N} \ln \frac{N_i}{N}$, where N_i are the numbers of molecules
Heat transfer	$dS = \left(\frac{1}{T_1} - \frac{1}{T_2}\right) dQ$, where T_1 and T_2 are the temperatures of the two bodies

$$dQ = \mu W dx \tag{2.48}$$

The rate of entropy generation during friction is now given by

$$\frac{dS}{dt} = \frac{\mu WV}{T} \tag{2.49}$$

with the flow rate $J = V$ and the thermodynamic force $X = \mu W/T$ [15].

Bryant et al. [100] suggested a degradation measure w that is a parameter associated with a particular degradation mechanism, so that the rate of degradation is given by

$$\frac{dw}{dt} = B\frac{dS_f}{dt} = YJ \tag{2.50}$$

where $Y = BX$ is the generalized degradation force and B is a constant degradation coefficient (a material property).

For the wear process, it is natural to take wear volume as the degradation measure w [15]. Using the relation between the degradation rate $\dot{w} = B\dot{S}$ and entropy rate, we obtain the wear rate

$$\frac{dw}{dt} = B\frac{\mu WV}{T} \tag{2.51}$$

For plastic contact, (2.47) can be rewritten by setting the wear coefficient $k = \mu HB/T$ as

$$\frac{dw}{dt} = k\frac{WV}{H} \tag{2.52}$$

where H is the hardness of a softer material in contact. This is the Archard equation for adhesive wear. For elastic contact, $k = \mu E^*(\sigma/\beta^*)B/T$ yields

$$\frac{dw}{dt} = k\frac{WV}{E^*(\sigma/\beta^*)} \tag{2.53}$$

where E^* is the effective elastic modulus, σ is the standard deviation of rough profile height, and β^* is the correlation length of profile roughness (in a sense, σ is the height, and β^* is the length of a typical asperity) [15].

The nontrivial part of this derivation is that the wear volume per unit time is linearly proportional to the friction force. This implies that (a) a constant value of energy dissipated by friction is consumed for wear debris generation and (b) a constant amount of energy is consumed, in average per wear particle volume. Wear and friction are essentially the same dissipative process, as the energy consumed for creating wear particles is related to the work of friction. The model, however, cannot predict actual values of the wear coefficients, and its advantage is in providing theoretical foundation of the empirical laws of wear.

A different approach was taken by Fedorov [101], who pointed out that thermodynamically wear is an irreversible mass transfer process dependent upon the local gradients of chemical potentials. The balance of energy in a tribo-system is given by

$$\rho \mathrm{TdS} = \rho \mathrm{dU} - \sigma_{\mathrm{ik}} \cdot \mathrm{d}\overline{\varepsilon}_{\mathrm{ik}} - \mathrm{N_j d}\mu_{\mathrm{i}} \tag{2.54}$$

where ρ is the density and σ_{ik} and $\overline{\varepsilon}_{\mathrm{ik}}$ are the stress and strain tensors. The mass transfer in a frictional system depends upon the heat flow, dissipation, and chemical potentials of components in the system.

According to Fedorov, the probability of deterioration is proportional to the exponent of the entropy flow and relaxation time τ, which characterizes the process of restoring the thermodynamic equilibrium

$$\omega \propto \exp\left(\frac{\dot{S}\tau}{k}\right) \tag{2.55}$$

The hidden energy of degradation is created by the fluctuation of thermal energy in the mechanical stress field. When the hidden energy reaches its critical density, the destruction occurs. The hidden area density as a function of time for steel is shown in Fig. 2.14 for the values of stress s = (25.3, 24.8, 23.9, 23.1, 22.5) kg/mm^2.

It is of interest also to consider the model, suggested by Bershadsky [102], who also believed that friction and wear are related processes that represent the trend to deteriorate for energy and matter, respectively. Bershadsky [102] introduced the concept of structural adjustment. During the structural adjustment, all types of interactions (adhesion, deformation, and material transfer are localized at the

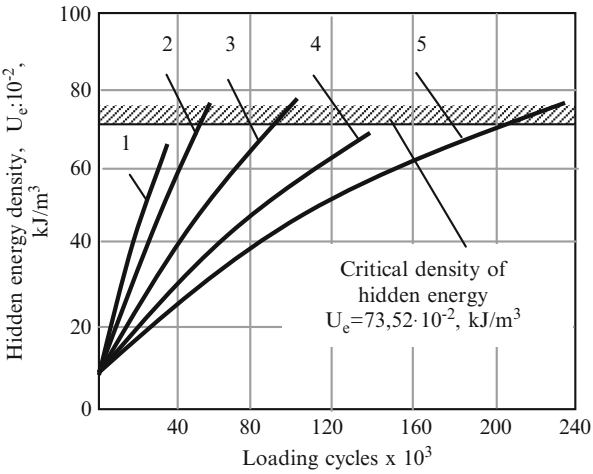

Fig. 2.14 Variation of hidden energy density with loading cycles (Berkovich and Gromakovsky, 2000)

surface), which decreases the absorbed energy ΔE in the work of friction A = ΔE + Q. Bershadsky [102] formulated the variational principle

$$\delta \int_V \frac{\Delta E(V)}{A} dV = 0 \tag{2.56}$$

According to this principle, most work is converted into heat. Dissipative ability of the material, along with its hardness, defines the wear resistance.

To summarize, the thermodynamic theories of wear provide foundation for the empirical wear laws (such as the Archard law) and suggest the principles to calculate the parameters of these laws (such as the wear coefficient).

3.3 *Factors Affecting Wear*

It is well known that no single wear mechanism operates over a wide range of operating conditions. The transitions in dominant wear mechanisms occur as operating conditions are changed. In this regard, efforts were made to develop wear mechanism maps [103]. The wear mechanism map shows various regimes of wear at wide operating conditions.

Normal load: Increasing the normal load results in an increase in the real area of contact and hence the number of adhesive junctions. In general, it is stated that the wear loss is proportional to applied normal load during sliding [40]. Archard [94] observed the transition from mild to severe wear, when the contact pressure is about one-third of hardness of metals. This is due to interaction of plastic zones beneath the contacting asperities. In high load regime, mechanical damage of material occurs due to high surface stresses. Also increase in load results in monotonic increase in

interface temperature, which reduces the yield stress of a material. Hence, it is clear that wear rate of material is linear function of normal load. However, rate of increase in wear rate does not remain constant over range of normal load.

Sliding velocity: In dry sliding condition, with increasing sliding speed, the frictional heat generated becomes greater causing oxidation and forms an oxide film at the interface. This oxide film serves as lubricant which reduces the wear rate of metals. In the case of lubricated condition, at higher sliding speed, the formation of hydrodynamic lubricant film at the interface minimizes the wear rate. Normally, wear rate of metals decreases with sliding speed both in dry and lubricated sliding conditions [104]. However, if interfacial temperature reaches the melting point of a metal, it lowers the hardness of the metals drastically and causes severe wear.

Temperature: The temperature is an important parameter which influences the wear response of metals by accelerating the chemical reactivity of a metal surface, altering the physical and mechanical properties of the metals and changing the microstructural response of the metals. To study the effect of temperature, sliding tests were performed on cobalt–steel pair at different temperatures. It was noted that wear rate at 653 K is about 100 times than that observed at 553 K. The reason is due to phase transformation from HCP to FCC structure [40].

Environment: In ambient conditions, an oxide film is easily formed on metal surface, and if oxide film is strong enough to prevent the direct contact between metal–metal surfaces, wear rate of metals will be low as compared to inert atmosphere. One could expect that wear rate of metals is higher in vacuum than in air owing to the less chance of formation of oxide films. This leads to direct metal–metal contact and results in high wear.

Hardness: Archard's model considers wear rate of metals as an inverse function of their hardness. Harder materials resist cutting and penetration. In the case of abrasive wear, it is easy to correlate hardness with wear rate as it involves penetration process.

Elastic modulus: The wear resistance of a material is directly related to elastic modulus in accordance with adhesive theory of wear [105]. For metals that have high elastic modulus decrease the real area of contact leading to low adhesion and wear. The abrasive wear resistance of a material can also be varied by varying hardness/modulus ratio (i.e., H/E ratio). The ratio shows that abrasive wear resistance of a material can be increased either by increasing the hardness or by decreasing the elastic modulus.

Fracture toughness: The high fracture toughness increases the wear resistance of brittle materials such as ceramics. During interaction of asperities, crack growth occurs with critical amount of strain. If the applied strain is smaller than critical strain, the wear rate of a metal is independent of fracture toughness. Once the critical strain is reached, there is an increased probability of crack growth and wear rate of metals depends upon the fracture toughness. Hornbogen [106] proposed a model that there are three regions of wear behavior as a function of fracture toughness. In the first region, wear is not affected by toughness in which Archard's

law is obeyed. Second region involves transition from mild to severe wear. Factors which induce the transition are an increased pressure, strain rate, and decreased fracture toughness. Third region is highly brittleness condition which shows high wear rate because of low fracture toughness.

Crystal structure: Sliding of metals produces large plastic deformation, which in turn forms dislocation cell wall structures near the surface region. Since cell walls serve as pathway for subsurface cracks, metals with limited number of slip systems (HCP) exhibit lower wear rate than metals with large number of slip systems (FCC). Buckley [107] showed experimentally that cubic crystals wear at about twice the rate of hexagonal crystals.

Thermal diffusivity: If a metal has low thermal diffusivity, it cannot dissipate the frictional heat away from the interface. This thermal accumulation degrades the mechanical strength of a metal and causes high wear. Wear is an inverse function of thermal diffusivity. Abdel-Aal [108] related the heat dissipation capacity of metals with wear transition. He postulated that transition from mild to severe wear occurs once the quantity of heat generated is higher than the quantity of heat dissipated. He also noted that if the amount of thermal accumulation reaches a critical value, delamination of oxide flake results in higher wear rate.

3.4 Role of Subsurface Zone on Wear

Sliding of metals produces large plastic deformation at the interface and there exist large strain gradients in the near-surface zone. The structure and properties of such zones are central to the formation of wear debris, since they come out directly from the near-surface zone.

Prior to the introduction of the delamination theory, a unifying thread to gain insight into the basis of wear was less apparent. However, Suh's theory [39] requires an examination of subsurface region of wear specimens, and hence, investigators began to study the mechanics of deformation and crack nucleation beneath the wear interface.

To study the subsurface features following a sliding test, specimens were sectioned perpendicular to a worn surface and along the sliding direction and then polished and examined. Figure 2.15 shows, schematically, the major features observed in a section of the specimen after a wear test. These are characteristic subsurface zones, which depend (morphologically and compositionally) upon specimen/counterface materials and geometry, the environment, and the mechanical conditions of contact. In Fig. 2.15, zone 1 represents original specimen material in an undisturbed state. That is, this zone experiences elastic deformation and thermal cycling when loaded during tribo-contact. However, the structure and properties of zone 1 following a sliding test are similar to those prior to the test. But unlike zone 1, the zone 2 material has acquired new structure and properties due to repetitive tribo-contact, and considerable plastic deformation occurs in ductile

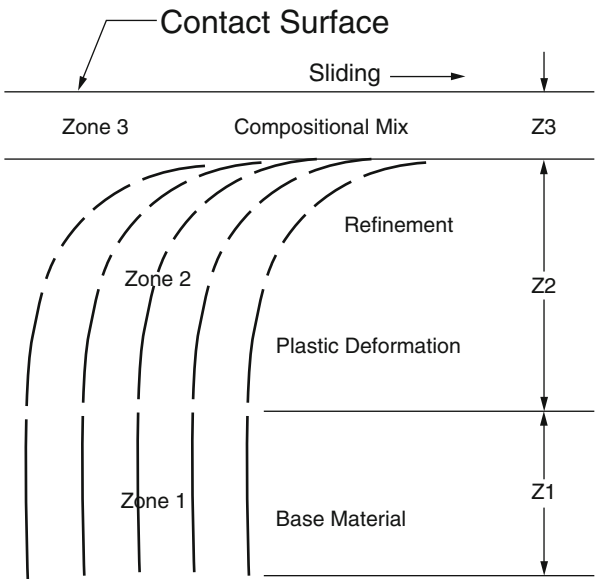

Fig. 2.15 A schematic diagram of subsurface zones observed beneath wear surfaces

materials. Depending upon the materials, environment, and contact conditions, zone 2 may become harder or softer than the original material. Voids may develop within zone 2, and cracks may nucleate within this region. In many cases the reorientation and disintegration of crystallites are observed in zone 2, with attendant refinement in microstructure that increases as the contact interface is approached. However, in zone 2, no constituents from the counterface or stemming from interaction with the environment are present. The extent of deformation in zone 2 ranges from zero at the zone 1 to zone 2 interface to a maximum at the zone 2 to zone 3 interface. Zone 3 is a tribo-layer which forms in situ. Zone 3 is the region containing the surface of contact, and it commonly differs compositionally as well as morphologically from the base material (zones 1 and 2). Often, zone 3 appears to be homogeneous and very finely structured consisting of both the specimen and counterface material, as well as constituents from the operating environment. In single-phase materials it is difficult to quantify the extent of deformation while the use of suitable two phase alloys enabled measurement of the depth of damage from the structural changes that result [109].

Origin of subsurface zone: The development of a subsurface zone involves several stages. During initial stage of sliding, the forces acting on the sliding surface are transmitted to the subsurface zone. The tangential shear forces induced by the frictional contact between contacting asperities tend to deform the near-surface material plastically. The frictional force increases with sliding distance until it reaches a steady value. At this steady-state sliding, the subsurface material is subjected to plastic deformation of considerable stable depth. In addition, crack-like elongated voids appear within the plastic zone due to the presence of secondary phase particles in the metal matrix. These cracks tend to propagate and link up with

adjacent cracks to produce loose wear debris in the near-surface material. When the surface layers are removed, material in the lower region of zone 2 comes into high strain region and finally becomes zone 3. In the same manner, the material in the zone 3 enters into zone 2. The depth of plastic deformed zone remains constant during subsequent removal of surface material in sliding wear.

3.5 Strain Rate Response Approach

Wear is a dynamic process and its behavior can be related to the strain rate response of a material. A strain rate response approach is associated with microstructural responses of metals to imposed conditions of strain, strain rate, and temperature. Depending on the combination of strain rate and temperature, various kinds of microstructural mechanisms will operate leading to different microstructure. The microstructural response is mainly based on dynamics material modeling (DMM) [110]. DMM is based upon the principle that the efficiency by which material dissipates power decides its microstructural response. The power involved during plastic deformation is given by $P = \sigma\dot{\varepsilon}$, where σ is the flow stress and $\dot{\varepsilon}$ is the applied strain rate. According to DMM, this power is consumed in heat dissipation and microstructural changes. This power partitioning is decided by strain rate sensitivity of flow stress (m) of the material. The efficiency in utilizing the power in undergoing microstructural change decides the microstructural response of material. The material when subjected to various conditions of strain, strain rate, and temperature exhibits a large spectrum of microstructural responses. The various microstructural responses of materials include dynamic recrystallization (DRX), dynamic recovery (DRY), adiabatic shear banding (ASB), flow banding (FB), wedge cracking (WC), void formation (VF), superplastic deformation (SPD), intercrystalline cracking (ICC), and prior particle boundary (PPB) cracking. Some of these like DRX, DRY, and SPD microstructure evolution lead to desirable microstructure, and the others like ASB, FB, WC, VF, PPB, and ICC can lead to undesirable microstructure that destroys the integrity of the material. For a given metal or alloy, the specific microstructural evolution was found to be related to the imposed strain rate and temperature and therefore designated as strain rate response. This frame of work may be extended to a wear situation, as in the subsurface regions a large gradient of strain exists [78, 111]. This, during sliding, means that a particular combination of strain rate and temperature exists at the surface and the near-surface regions where plastic deformation is occurring. In such a situation, the regions where the strain rate and temperature combination is such that a deleterious strain rate response may occur, it will be easier for cracks to be nucleated and propagated, thus generating wear debris. Figure 2.16 shows the strain rate microstructural response map for titanium obtained from the uniaxial compression tests done at various constant true strain rates and temperatures. The curves represent the strain rates and temperatures estimated in the subsurface of the titanium pin at various sliding speeds and depths. In case of titanium, Kailas and

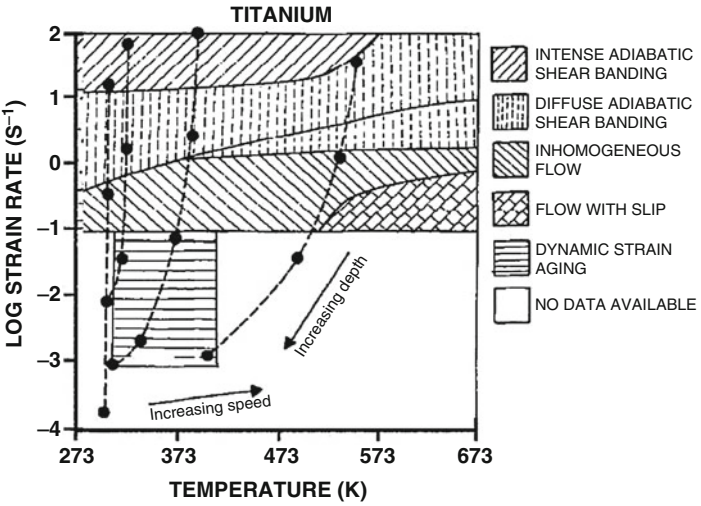

Fig. 2.16 Strain rate microstructural response map for titanium [113]

Biswas [112] observed experimentally that wear rate reduces with an increase in sliding speed. This was postulated to be due to the reduction in the intensity of ASB (microstructural instability) in near-surface regions of the titanium pin. Strain rate response approach made a good correlation between the wear rate and microstructural evolution in the near-surface region [113].

3.6 Wear of Materials

Wear is a complex phenomenon. Wear rate may vary with time or sliding distance. Also, wear rate may vary if transition from one mechanism to another occurs during the wear process. The initial period during which wear rate changes is known as the run-in period. Wear during run-in depends on the initial material properties and surface conditions. During the transition period, the surface is modified to a steady-state condition by plastic deformation. The wear rate, like friction of a material, is dependent on the mating materials, surface finish, and operating conditions.

Metals and alloys: Under dry condition, clean metals and alloys exhibit high adhesion and thus high friction and wear. In vacuum, wear rate of metallic materials is very high. Under lubricated conditions or in the presence of chemical films, metals and alloys exhibit low adhesion and thus the friction and wear. In soft metals, such as Pb and Sn, the real area of contact is high, even at light loads, which results in high wear rates. Hexagonal (HCP) metals such as Mg and Zn exhibit low friction and wear when compared to FCC metals. In general, wear for alloys tends to be lower than that of pure components.

Ceramics: Ceramic–ceramic or ceramic–metal exhibits moderate friction but extremely low wear. This is due to high mechanical properties of ceramics which result in very low real area of contact responsible for low friction and wear. Under clean environment, coefficient of friction and wear rates of ceramic pair do not reach the very high values as observed in clean metals, especially in ultra-high vacuum. Ceramic materials respond to conventional lubricants similar to metals.

Polymers: Polymers generally exhibit low friction and moderates wear as compared to metals and ceramics. Dominant wear mechanisms are adhesive, abrasive, and fatigue. If the mating surfaces are smooth, then the wear primarily occurs from adhesion. If the mating surfaces are rough, then the wear is due to abrasion. The fatigue mechanism is important in harder polymers sliding against smooth surfaces. In this case, asperity deformations are primarily elastic and wear due to fatigue results from the formation of cracks associated with predominantly elastic deformation. Wear particles are produced by propagation and intersection of cracks. Polymers flow readily at modest pressure and temperature. Therefore, polymers are used at relatively low loads, speed, and temperatures, lower than that in the case of metals and ceramics. Polymers generally have low thermal conductivities and thus high interface temperature during sliding. Sometimes, polymers start to melt at the interface even at ambient temperature and hence the wear rate increases rapidly.

3.7 Correlation Between Friction and Wear

As explained earlier, friction and wear are not intrinsic material properties, but they are a responsive of tribo-system. These processes are not always linearly related to each other and assuming so would be erroneous. One could expect that high friction coefficients are correlated with high wear rates. Friction and wear, as two kinds of responses from one tribo-system, could be exactly related with each other in each state of contact in the system, although a comprehensive simple relationship should not be obtained. Kato [114] suggested that it would be helpful for the understanding of the relationship between friction and wear by describing the tribo-system with respective terms of hardness, ductility, oxide film layer, and adhesive transfer. The mathematical relation between friction coefficient and wear rate for the case of sliding wear was formulated based on delamination theory of wear and energy criteria [115]. According to this model, friction and wear coefficients are related to each other by material properties and are proportional to each other in normal range of sliding condition.

4 Conclusions

Friction is very important in our day-to-day lives. Many techniques have been used to control, decrease, or increase friction based on applications. In this chapter, the fundamentals of friction and wear are presented. More specifically, the empirical

laws, mechanisms, and factor affecting friction and wear were discussed. Friction measuring devices, friction and wear studies of various materials, and the correlation between friction and wear were also discussed.

References

1. Menezes PL, Kishore, Kailas SV, Lovell MR (2011) Response of materials during sliding on various surface textures. J Mater Eng Perform 20(8):1438–1446
2. Menezes PL, Kishore, Kailas SV (2008) Role of surface texture and roughness parameters in friction and transfer layer formation under dry and lubricated sliding conditions. Int J Mater Res 99(7):795–807
3. Nosonovsky M, Bhushan B (2008) Multiscale dissipative mechanisms and hierarchical surfaces: friction, superhydrophobicity, and biomimetics. Springer, Heidelberg
4. Adams GG, Barber JR, Ciavarella M, Rice JR (2005) A paradox in sliding contact with friction. ASME J Appl Mech 72:450–452
5. Adams GG (1995) Self-excited oscillations of two elastic half-spaces sliding with a constant coefficient of friction. ASME J Appl Mech 62:867–872
6. Nosonovsky M, Adams GG (2004) Vibration and stability of frictional sliding of two elastic bodies with a wavy contact interface. ASME J Appl Mech 71:154–161
7. Adams GG, Nosonovsky M (2000) Contact modeling—forces. Tribol Int 33:441–442
8. Nosonovsky M, Adams GG (2001) Dilatational and shear waves induced by the frictional sliding of two elastic half-spaces. Int J Eng Sci 39:1257–1269
9. Tolstoi DM (1967) Significance of the normal degree of freedom and natural normal vibrations in contact friction. Wear 10:199–213
10. Persson BNJ (2000) Sliding friction: physical principles and applications. Springer, Berlin
11. Rice JR, Lapusta N, Ranjith K (2001) Rate and state dependent friction and the stability of sliding between elastically deformable solids. J Mech Phys Solids 49:1865–1898
12. Nosonovsky M (2007) Modeling size, load, and velocity effect on friction at micro/nanoscale. Int J Surf Sci Eng 1:22–37
13. Barber JR (1969) Thermoelastic instabilities in the sliding of conforming solids. Proc R Soc Lond A 312:381–394
14. Fox-Rabinovich GS, Totten GE (eds) (2006) Self-organization during friction. CRC, Boca Raton, FL
15. Nosonovsky M, Bhushan B (2009) Thermodynamics of surface degradation, self-organization, and self-healing for biomimetic surfaces. Philos Trans R Soc A 367:1607–1627
16. Menezes PL, Kishore, Kailas SV (2009) Studies on friction and formation of transfer layer when Al-4Mg alloy pins slid at various numbers of cycles on steel plates of different surface texture. Wear 267(1–4):525–534
17. Menezes PL, Kishore, Kailas SV, Lovell MR (2010) "Studies on friction and transfer layer formation when pure Mg pins slid at various numbers of cycles on steel plates of different surface texture." ASME/STLE international joint tribology conference (IJTC2010) San Francisco, USA, pp 263–265
18. Menezes PL, Kishore, Kailas SV, Lovell MR (2011) The role of surface texture on friction and transfer layer formation during repeated sliding of Al-4Mg against steel. Wear 271(9–10):1785–1793
19. Menezes PL, Kishore, Kailas SV, Lovell MR (2012) "Self-organization and friction during sliding." ASME/STLE international joint tribology conference (IJTC2012), Denver, USA
20. Menezes PL, Kishore, Kailas SV, Lovell MR (2013) Tribological response of soft materials sliding against hard surface textures at various numbers of cycles. Lubrication Sci 25 (2):79–99

21. Mortazavi V, Menezes PL, Nosonovsky M (2011) Studies of Shannon entropy evolution due to self-organization during the running-in. ASME/STLE international joint tribology conference (IJTC2011), Los Angeles, USA, pp 303–305
22. Menezes PL, Kishore, Kailas SV, Lovell MR (2010) Studies on friction and transfer layer formation when high purity Al pins slid at various numbers of cycles on steel plates of different surface texture. Proceedings of the 2010 STLE annual meeting & exhibition, Las Vegas, USA
23. Menezes PL, Kishore, Kailas SV, Lovell MR (2010) Role of surface texture on friction and transfer layer formation when pure Al pins slid at various numbers of cycles on steel plates. 2011 STLE annual meeting & exhibition, Atlanta, USA
24. Bhushan B, Nosonovsky M (2003) Scale effects in friction using strain gradient plasticity and dislocation-assisted sliding (microslip). Acta Mater 51:4331–4345
25. Carpinteri A, Paggi M (2005) Size-scale effect on the friction coefficient. Int J Solid Struct 42:2901–2910
26. Niederberger S, Gracias DH, Komvopoulos K, Somorjai GA (2000) Transition from nanoscale to microscale dynamic friction mechanisms on polyethylene and silicon surfaces. J Appl Phys 87:3143–3150
27. Zhang LC, Johnson KL, Cheong WCD (2001) A molecular dynamics study of scale effects on the friction of single-asperity contacts. Tribol Lett 10:23–28
28. Wenning L, Müser MH (2001) Friction laws for elastic nanoscale contacts. Europhys Lett 54:693–699
29. Nosonovsky M (2009) From wear to self-healing in nanostructured biological and technical surfaces. Proceedings of ASME/STLE international joint tribology conference IJTC2009, Memphis, USA, ASME
30. Bowden FP, Tabor D (1950) The friction and lubrication of solids, Part-I. Clarendon, UK
31. Rice J (1991) Dislocation nucleation from a crack tip: an analysis based on the peierls concept. J Mech Phys Solids 40:239–271
32. Gerde E, Marder M (2001) Friction and fracture. Nature 413:285–288
33. Kessler DA (2001) Surface physics: a new crack on friction. Nature 413:260–261
34. Chang WR, Etzion I, Bogy DB (1987) An elastic-plastic model for the contact of rough surfaces. ASME J Tribol 109:257–263
35. Kogut L, Etsion I (2004) A static friction model for elastic-plastic contacting rough surfaces. ASME J Tribol 126:34–40
36. He G, Müser MH, Robbins MO (1999) Adsorbed layers and the origin of static friction. Science 284:1650–1652
37. Greenwood JA, Williamson JBP (1966) Contact of nominally flat surfaces. Proc R Soc Lond A 295:300–319
38. Archard JF (1957) Elastic deformation and the laws of friction. Proc R Soc Lond A 243:190–205
39. Suh NP (1986) Tribophysics. Prentice-Hall, Inc, Englewood Cliffs, NJ
40. Rabinowicz E (1995) Friction and wear of materials. Wiley, USA
41. Kudo H (1965) A note on the role of microscopically trapped lubricant at the tool-work interface. Int J Mech Sci 7(5):383–388
42. Staph HE, Ku PM, Carper HJ (1973) Effect of surface roughness and surface texture on scuffing. Mech Mach Theor 8:197–208
43. Koura MM (1980) The effect of surface texture on friction mechanisms. Wear 63(1):1–12
44. Lakshmipathy R, Sagar R (1992) Effect of die surface topography on die-work interfacial friction in open die forging. Int J Mach Tool Manuf 32(5):685–693
45. Saha PK, Wilson WRD, Timsit RS (1996) Influence of surface topography on the frictional characteristics of 3104 aluminum alloy sheet. Wear 197(1–2):123–129
46. Hu ZM, Dean TA (2000) A study of surface topography, friction and lubricants in metal forming. Int J Mach Tool Manuf 40(11):1637–1649

47. Rasp W, Wichern CM (2002) Effects of surface-topography directionality and lubrication condition on frictional behaviour during plastic deformation. J Mater Process Technol 125–126:379–386
48. Menezes PL, Kishore, Kailas SV (2006) Studies on friction and transfer layer: role of surface texture. Tribol Lett 24(3):265–273
49. Menezes PL, Kishore, Kailas SV, Lovell MR (2009) Studies on friction and formation of transfer layer in HCP metals. ASME J Tribol 131(3):031604.1–031614.9
50. Menezes PL, Kishore, Kailas SV, Bobji MS (2010) Influence of tilt angle of plate on friction and transfer layer - A study of aluminium pin sliding against steel plate. Tribol Int 43(5–6):897–905
51. Menezes PL, Kishore, Kailas SV, Lovell MR (2012) Analysis of strain rates and microstructural evaluation during metal forming: role of surface texture and friction. Tribol Trans 55(5):582–589
52. Kumar PC, Menezes PL, Kailas SV (2008) Role of surface texture on friction under boundary lubricated conditions. Tribol Online 3(1):12–18
53. Gadelmawla ES, Koura MM, Maksoud TMA, Elewa IM, Soliman HH (2002) Roughness parameters. J Mater Process Technol 123(1):133–145
54. Menezes PL, Kishore, Kailas SV (2006) Influence of surface texture on coefficient of friction and transfer layer formation during sliding of pure magnesium pin on 080 M40 (EN8) steel plate. Wear 261(5–6):578–591
55. Menezes PL, Kishore, Kailas SV (2008) Effect of surface roughness parameters and surface texture on friction and transfer layer formation in tin-steel tribo-system. J Mater Process Technol 208(1–3):372–382
56. Menezes PL, Kishore, Kailas SV (2006) Effect of roughness parameter and grinding angle on coefficient of friction when sliding of Al-Mg alloy over EN8 steel. ASME J Tribol 128(4):697–704
57. Menezes PL, Kishore, Kailas SV (2008) Influence of roughness parameters on coefficient of friction under lubricated conditions. Sadhana 33(3):181–190
58. Menezes PL, Kishore, Kailas SV (2009) Influence of surface texture and roughness parameters on friction and transfer layer formation during sliding of aluminium pin on steel plate. Wear 267(9–10):1534–1549
59. Menezes PL, Kishore, Kailas SV, Lovell MR (2011) Influence of inclination angle and machining direction on friction and transfer layer formation. ASME J Tribol 133(1):014501.1–014501.8
60. Menezes PL, Kishore, Kailas SV, Lovell MR (2011) Friction and transfer layer formation in polymer-steel tribo-system: Role of surface texture and roughness parameters. Wear 271(9–10):2213–2221
61. Pottirayil A, Menezes PL, Kailas SV (2010) A parameter characterizing plowing nature of surfaces close to Gaussian. Tribol Int 43(1–2):370–380
62. Pottirayil A, Menezes PL, Kailas SV (2008) Correlating the features of topography to friction by sliding experiments. Proceedings of the 9th biennial ASME conference on engineering systems design and analysis (ESDA 2008), Israel, pp 361–364
63. Menezes PL, Kishore, Kailas SV (2006) Studies on friction and transfer layer using inclined scratch. Tribol Int 39(2):175–183
64. Menezes PL, Kishore, Kailas SV (2008) On the effect of surface texture on friction and transfer layer formation—a study using Al and steel pair. Wear 265(11–12):1655–1669
65. Menezes PL, Kishore, Kailas SV (2009) Influence of inclination angle of plate on friction, stick-slip and transfer layer—a study of magnesium pin sliding against steel plate. Wear 267(1–4):476–484
66. Menezes PL, Kishore, Kailas SV (2006) Effect of directionality of unidirectional grinding marks on friction and transfer layer formation of Mg on steel using inclined scratch test. Mater Sci Eng A 429(1–2):149–160

67. Menezes PL, Kishore, Shimjith M, Kailas SV (2007) Influence of surface texture on friction and transfer layer formation in Mg-8Al alloy/steel tribo-system. Indian J Tribol 2(1):46–54
68. Menezes PL, Kishore, Kailas SV (2008) Influence of roughness parameters of harder surface on coefficient of friction and transfer layer formation. Int J Surf Sci Eng 2(1–2):98–119
69. Menezes PL, Kishore, Kailas SV (2009) Influence of roughness parameters and surface texture on friction during sliding of pure lead over 080 M40 steel. Int J Adv Manuf Technol 43(7):731–743
70. Menezes PL, Kishore, Kailas SV (2009) Study of friction and transfer layer formation in copper-steel tribo-system. Tribol Trans 52(5):611–622
71. Menezes PL, Kishore, Kailas SV, Lovell MR (2011) Role of surface texture, roughness and hardness on friction during unidirectional sliding. Tribol Lett 41(1):1–15
72. Buckley DH, Johnson RL (1968) The influence of crystal structure and some properties on hexagonal metals on friction and adhesion. Wear 11(6):405–419
73. Menezes PL, Kishore, Kailas SV, Lovell MR (2012) 'Tribological response of materials with varying hardness and crystal structure during sliding on various surface textures. Materials and Surface Engineering: Research and Development, Woodhead, pp 207–242
74. Menezes PL, Kishore, Kailas SV, Lovell MR (2010) Response of materials as a function of grinding angle on friction and transfer layer formation. Int J Adv Manuf Technol 49(5):485–495
75. Menezes PL, Kishore, Kailas SV, Lovell M R (2011) Factors influencing stick-slip motion: Effect of hardness, crystal structure and surface texture. ASME/STLE international joint tribology conference (IJTC2011), Los Angeles, USA, 2011, pp 71–73
76. Menezes PL, Kishore, Kailas SV, Lovell MR (2012) Tribological response of materials with varying hardness and crystal structure during sliding on various surface textures. Materials and Surface Engineering: Research and Development, Woodhead, pp 207–242
77. Menezes PL, Kishore, Kailas SV (2008) Subsurface deformation and the role of surface texture—a study with Cu pins and steel plates. Sadhana 33(3):191–201
78. Menezes PL, Kishore, Kailas SV (2009) Role of surface texture of harder surface on subsurface deformation. Wear 266(1–2):103–109
79. Moore MA, King FS (1980) Abrasive wear of brittle solids. Wear 60(1):123–140
80. Menezes PL, Kishore, Kailas SV (2008) Effect of surface topography on friction and transfer layer during sliding. Tribol Online 3(1):25–30
81. Menezes PL, Kishore, Kailas SV, Lovell MR (2013) The role of strain rate response on tribological behavior of metals. ASME J Tribol 135(1):011601.1–011601.7
82. Miyoshi K (1990) Fundamental considerations in adhesion, friction and wear for ceramic-metal contacts. Wear 141(1):35–44
83. Farhat ZN, Ding Y, Northwood DO, Alpas AT (1996) Effect of grain size on friction and wear of nanocrystalline aluminum. Mater Sci Eng A 206(2):302–313
84. Bregliozzi G, Schino AD, Kenny JM, Haefke H (2003) The influence of atmospheric humidity and grain size on the friction and wear of AISI 304 austenitic stainless steel. Mater Lett 57(29):4505–4508
85. Wang ZB, Taao NR, Li S, Wang W, Liu G, Lu J, Lu K (2003) Effect of surface nano-crystallization on friction and wear properties in low carbon steel. Mater Sci Eng A 352(1–2):144–149
86. Mishra R, Basu B, Balasubramaniam R (2004) Effect of grain size on the tribological behavior of nanocrystalline nickel. Mater Sci Eng A 373(1–2):370–373
87. Whitehead JR (1950) Surface deformation and friction of metals at light loads. Proc R Soc Lond A 201:109–124
88. Bowden FP, Young JE (1951) Friction of clean metals and the influence of adsorbed films. Proc R Soc Lond A 208:311–325
89. Tsuya Y (1975) Microstructure of wear, friction and solid lubrication. Tech. Rep. of Mech. Eng. Lab. 3(81), Japan

90. Menezes PL, Kishore, Kailas SV, Lovell MR (2011) Studies on friction in steel-aluminum alloy tribo-system: role of surface texture of the softer material. 2011 STLE annual meeting & exhibition, Atlanta, USA
91. Menezes PL, Kishore, Kailas SV, Lovell MR (2009) Influence of alloying element addition on friction and transfer layer formation in Al-Mg system: role of surface texture. Proceedings of ASME/STLE international joint tribology conference IJTC2009, Memphis, USA, ASME, 2009, pp 459-461
92. Menezes PL, Kishore, Kailas SV, Lovell MR (2010) Response of metals and polymers during sliding: Role of surface texture. ASME/STLE international joint tribology conference (IJTC2010), San Francisco, USA, 2010, pp 267–269
93. Menezes PL, Kishore, Kailas SV, Lovell MR (2010) Role of surface texture on friction and transfer layer formation during sliding of PVC pin on steel plate. Proceedings of the 2010 STLE annual meeting & exhibition, Las Vegas, USA, 2010
94. Archard JF (1953) Contact and rubbing of flat surfaces. J Appl Phys 24(8):981–988
95. Suh NP (1973) The delamination theory of wear. Wear 25(1):111–124
96. Klamecki BE (1980) Wear—an entropy production model. Wear 58(2):325–330
97. Zmitrowicz A (1987) A thermodynamical model of contact, friction, and wear. Wear 114(2):135–221
98. Bryant MD (2009) Entropy and dissipative processes of friction and wear. FME Trans 37:55–60
99. Doelling KL, Ling FF, Bryant MD, Heilman BP (2000) An experimental study of the correlation between wear and entropy flow in machinery components. J Appl Phys 88 (5):2999–3003
100. Bryant MD, Khonsari MM, Ling FF (2008) On the thermodynamics of degradation. Proc R Soc Lond A 464(2096):2001–2014
101. Berkovich II, Gromakovsky DG (2000) Tribology: physical fundamentals, mechanical and technical applications. Samara, Russia
102. Bershadski LI (1993) B I Kostetski and the general concept in tribology. Trenie I Iznos 14:6–18
103. Lim SC, Ashby MF (1987) Overview no. 55 wear-mechanism maps. Acta Metal 35(1):1–24
104. Saka N, Eleiche AM, Suh NP (1977) Wear of metals at high sliding speeds. Wear 44(1):109–125
105. Khruschov MM (1974) Principles of abrasive wear. Wear 28(1):69–88
106. Hornbogen E (1975) The role of fracture toughness in the wear of metals. Wear 33(2):251–259
107. Buckley DH (1978) The use of analytical surface tools in the fundamental study of wear. Wear 46(1):19–53
108. Abdel-Aal HA (2000) On the influence of thermal properties on wear resistance of rubbing metals at elevated temperatures. ASME J Tribol 122(3):657–660
109. Rice SL, Nowotny H, Wayne SF (1989) A survey of the development of subsurface zones in the wear of materials. Key Eng Mater 33:77–100
110. Prasad YVRK, Sasidhara S (1997) Hot working guide: a compendium of processing maps. ASM International, Materials Park, OH
111. Kailas SV, Biswas SK (1997) Strain rate response and wear of metals. Tribol Int 30:369–375
112. Kailas SV, Biswas SK (1995) The role of strain rate response in plane strain abrasion of metals. Wear 181–183:648–657
113. Kailas SV (2003) A study of the strain rate microstructural response and wear of metals. J Mater Eng Perform 12(6):629–637
114. Kato K (2000) Wear in relation to friction—a review. Wear 241(2):151–157
115. Suh NP, Sridharan P (1975) Relationship between the coefficient of friction and the wear rate of metals. Wear 34(3):291–299

Questions

1. Explain friction mechanisms. Calculate the friction coefficient when conical asperities slid against softer materials.
2. State empirical laws of friction. State and explain the adhesion theory of friction with suitable diagrams.
3. What are the factors affecting friction? Explain.
4. How does the crystal structure influence friction? Why do FCC metals have more friction than HCP metals?
5. Define wear. How do you measure wear?
6. Describe various wear mechanisms in detail.
7. What is adhesive wear? Derive Archard theory of adhesive wear.
8. What is abrasive wear? Derive the quantitative expression for abrasive wear.
9. Explain various subsurface zones that are formed during sliding.
10. What are the factors affecting wear process?
11. Explain the following:

    (a) Static and kinetic friction
    (b) Steady-state and stick–slip friction
    (c) Coefficient of friction and angle of friction
    (d) Real area and apparent area
    (e) Adhesion friction and plowing friction
    (f) Erosive wear and corrosive wear
    (g) Two-body wear and three-body wear
    (h) Fretting wear and fatigue wear

Problems

1. A steel ball is slid against an aluminum flat surface at two different normal loads. At low normal load, the coefficient of friction is 0.40 and the groove width is 0.4 mm. At high load, the coefficient of friction is 0.6 and the groove width is 0.8 mm. Calculate the adhesive component of friction. Given: $\mu_{total} = \mu_{adhesion} + \mu_{plowing}$.
2. A hard steel ball of 3 mm diameter slid against a soft aluminum surface, produces a groove of 1.5 mm width. Calculate the adhesive component of friction when coefficient of friction is recorded 0.4. Given: $\mu_{total} = \mu_{adhesion} + \mu_{plowing}$.
3. A steel surface with conical asperities of an average semi-angle of 60° slides against a soft aluminum surface of hardness, H = 100 MPa under a constant normal load of 20 N. Calculate the volume of aluminum displaced in unit slid distance.

4. A rigid cutter was used to cut a medium carbon steel bar of 5 mm diameter. The hardness of the carbon steel is 2 GPa. The width of cut is 0.5 mm. It took 5 min to cut and the energy expended was 50 W (Nm/s). The coefficient of friction between the cutter and the steel bar is 0.3. Calculate the wear coefficient of the steel bar during the cutting process.

Solutions

1. Given: $\mu_{total} = \mu_{adhesion} + \mu_{plowing}$
   For a ball on flat surface, the above equation can be rewritten as

$$\mu_{total} = \mu_{adhesion} + \frac{4r}{3\pi R} \tag{1}$$

   where 2r is the groove width and R is the radius of the steel ball.
   At low load, (1) can be written as

$$0.4 = \mu_{adhesion} + \frac{4 \times 0.2}{3\pi R} \tag{2}$$

   At high load, (1) becomes

$$0.6 = \mu_{adhesion} + \frac{4 \times 0.4}{3\pi R} \tag{3}$$

   Solving (2) and (3), we get $\mu_{adhesion} = 0.2$.

2. Given: $\mu_{total} = \mu_{adhesion} + \mu_{plowing}$
   For a ball on flat surface, the above equation can be rewritten as

$$\mu_{total} = \mu_{adhesion} + \frac{4r}{3\pi R} \tag{1}$$

   Here r = 0.75 mm and R = 1.5 mm.
   Solving (1), $0.4 = \mu_{adhesion} + \frac{4 \times 0.75}{3\pi \times 1.5}$,
   we get $\mu_{adhesion} = 0.18$.

3. Total volume of material displaced in unit sliding distance is given by

$$Q = \frac{2}{\pi} \frac{W}{H} \tan\theta.$$

Substituting values, we get

$$Q = \frac{2}{\pi} \times \frac{20}{100 \times 10^6} \tan 30 = 7.35 \times 10^{-8}.$$

4. We know that the total wear volume is given by

$$Q = K\frac{W}{H} \quad or \quad K = \frac{QH}{W}.$$

Wear volume of steel bar

$$Q = \frac{\pi d^2}{4} \times w$$

where w is the width of cut. Solving the parameters, we get

$$Q = \frac{\pi \times 0.005^2}{4} \times 0.5 \times 10^{-3} = 9.8 \times 10^{-9}$$

Work done is given by

$$F = Energy \times time$$

$$F = 50 \times 5 \times 60 = 15000$$

$$W = \frac{F}{\mu} = \frac{15000}{0.3} = 50000$$

$$K = \frac{QH}{W} = \frac{9.8 \times 10^{-9} \times 2 \times 10^9}{50000} = 3.9 \times 10^{-4}$$